Received April 7, 2020, accepted April 18, 2020, date of publication April 23, 2020, date of current version May 8, 2020.

Digital Object Identifier 10.1109/ACCESS.2020.2989777

Robust Centralized Control for DC Islanded Microgrid Considering Communication Network Delay

MUHAMMAD MEHDI, CHUL-HWAN KIM, (Senior Member, IEEE), AND MUHAMMAD SAAD, (Graduate Student Member, IEEE)

Department of Electrical and Computer Engineering, Sungkyunkwan University, Suwon 440-746, South Korea

Corresponding author: Chul-Hwan Kim (chkim@skku.edu)

This work was Supported by the National Research Foundation of Korea (NRF) grant funded by the Korean Government (MSIP) under Grant 2018R1A2A1A05078680.

ABSTRACT In recent years, the application of renewable energy resources (RES) with DC output has increased, and RES integration as DC islanded microgrids (DC ImGs) has attracted the attention of many researchers. However, DC ImGs face many challenges, and voltage stability is extremely critical for efficient power distribution. This challenge becomes more prominent when exogenous disturbances, as well as time-delay, exist in the system mainly because of the communication network. In this study, we develop a mathematical model of the time-delay DC ImG. To compensate for the effect of the time-delay, three control strategies are introduced—stabilizing, robust, and robust-predictor. The controller's stability is guaranteed based on the Lyapunov-Krasovskii theorem, whereas for the exogenous disturbance rejection, the $\mathcal{L}_2$-norm of the system is reduced. Furthermore, to obtain the proposed controllers' gains, linear-matrix-inequality constraints are formulated. The performances of the controllers are investigated through numerous simulations, and a detailed analysis is presented.

INDEX TERMS Centralized control, DC microgrid, Lyapunov-Krasovskii functional, prediction-based control, robust control, stabilizing control, time-delay system, voltage stability.

I. INTRODUCTION

The increasing use of DC loads and penetration of DC distributed generation units (DGUs) have attracted the attention of researchers worldwide [1], [2]. Therefore, in the recent years, the development of DC distribution systems and DC Microgrids [3] has attracted increasing attention. The integration of DC DGUs or sources to DC loads has several benefits. The two pronounced advantages are no requirement for synchronization and elimination of the DC/AC-AC/DC conversion losses between sources and loads [3]. Other benefits associated with the DC system are the absence of harmonics and reactive power flow controls. Additionally, the DC system is more economical in comparison with its AC counterpart [4], [5].

Despite the numerous advantages of DC systems, there are many power quality issues that cannot be ignored. For example, voltage control, current sharing or droop control, energy management, protection against faults, and system stability etc. are some of the challenges of DC system. However, in the presence of these challenges, it can be stated that the primary purpose of the DC system is the efficient integration of renewable energy resources (RESs) [1]–[3]. Moreover, DC systems are also extremely convenient for novel applications, such as electric aircrafts, spacecrafts, electric vehicles, naval ships, submarines, and data centers [6]–[10]. Inherently, most emerging applications are designed to be operated as DC islanded microgrids (DC ImGs). Hence, DC ImG is gaining the attention of researchers. Many researchers are currently working on the concept and application of an off-grid, stand-alone, self-sustained DC ImG based system [7], [11]–[13].

Typical microgrids (MGs) comprise renewable energy sources (RESs), which are also called DGUs. Storage units, and loads are also part of MGs. The DGUs may be solar PV systems, the storage units are either batteries or super-capacitors which have DC type output. The load can be a DC

The associate editor coordinating the review of this manuscript and approving it for publication was Xiaosong Hu.

or an AC load. In the case of DC microgrids (DCMGs), the components are interconnected via a DC Bus [5], [14], [15]. From the perspective of operation, a DCMG can be classified into two modes: grid-connected mode and islanded mode [5], [15]. In the grid-connected mode, the DCMG is connected to a utility grid via an AC/DC converter; therefore, it has a grid support. In the DC ImG, the system is operated as a stand-alone unit, i.e., it is not integrated with any DC or AC grid or infinite bus; hence, the control and voltage stabilities of the system become difficult to achieve.

Thus far, various control schemes have been proposed by researchers [16], such as centralized, distributed, hierarchical, and multi-agent based control schemes. Each scheme focuses on specific issues and suggests solutions. Voltage, current, time-delays, and droop are typical objectives of DCMG control schemes [12], [13], [17]–[19]. In addition to the basic control objectives, the control system can be designed achieve peculiar tasks such as optimal charging control for energy storage systems (ESS) for electric vehicles [20]. Furthermore, the cell equalization, temperature, operating constraints or the ESS can also be considered in the generalized predictive control system and passivity based hierarchical control system [21], [22], where, distributed average tracking approach and generalized predictive control are applied. Furthermore, as the communication system is almost ubiquitous [23], an increasing number of studies are proposing control schemes by exploiting the communication system. Previous studies [16], [24] have attempted to achieve more complex and advanced objectives through global communication coordinations. From the perspective of control and use of communication network topology, the DCMG can be generalized as follows [16], [24]:

1) *Centralized control*: The DGUs' states or data are shared with a centralized control terminal through dedicated communication links (DCLs), and the control signals are sent back using the same DCL [25]–[27].
2) *Decentralized control*: In this scheme, no DCLs exist. To control the DGUs, only local variables of the unit are required [7], [11], [13].
3) *Distributed control*: This scheme also requires DCLs. The DCLs are used to share information between the neighboring DGUs for coordination alone, whereas the local controllers serve as the control unit [28], [29]. Multiagent-based distributed control is a sub-category of this scheme [12], [19].
4) *Hierarchical control*: In this scheme, both local and central controllers are present. The communication between the local and central controllers is performed through a communication network. This is also known as a multi-level control scheme, where each level has a certain objective; for example, the local controllers are designed to maintain the voltage, and the centralized controller keeps a track of the system's energy requirements. In brief, more complex objectives can be achieved through this scheme [4], [30].

For the centralized control scheme, the MGs' essential information is collected for control operations. The centralized control scheme offers high controllability and observability. Moreover, it's implementation is simple and straightforward. Thus, it is a low-cost scheme. The major disadvantage of this scheme is the single point of failure. The control parameters are obtained offline; therefore, this scheme also lacks flexibility and expandability. Centralized control is preferred for systems with a fixed structure, where the data from all DGUs are shared with the centralized controller through a communication link. In MGs with decentralized controllers, each DGU is treated as a standalone unit and the local controller performs regulation by processing local data. Therefore, no surrounding DGU information is required for the operation of the system; hence, no real-time communication is required, which is a major advantage of decentralized schemes. However, because of the lack of coordination among DGU controllers, it is difficult to achieve a global objective [7], [11], [13]. The lack of coordination among the DGUs can be avoided by a distributed control scheme, wherein the DGUs share their local information and form a global consensus [29], [31]. In brief, the DGUs reach to an agreement and decision for operation and control purposes via consensus algorithms. For more complex tasks and higher intelligence, the distributed control scheme can be supported by a higher level centralized controller. Communication links are used for sharing data among levels.

Communication links in MG control induce delays, which affect the system stability. Previous studies have revealed that even a few milliseconds of delay can unfavorably deteriorate control performances, which may result in system instability [32], [33]. The communication delay in the system can vary randomly from tens to several hundreds of milliseconds or even more [34], [35]. Therefore, when designing an MG's controller, it is imperative to consider the communication delays in the control schemes and assure stability. However, despite the importance of delay, many recent studies have preferred not to consider it. Therefore, for zero communication delay cases, the stability of MG is not conclusive. The stability of MG in the presence of time-delay (TD) with a distributed control scheme is discussed in [28], [36], [37]. Furthermore, multiagent system (MAS)-based distributed coordinated control for a radial isolated system in [12], [19] also achieved voltage stability for the TD scenario. A complex three-level distributed control scheme is proposed in [38], where the system-level information is shared with the second-level control through a communication link with a delay. A simpler version of a hierarchical control scheme, i.e., master-slave based control, is applied in [33], [39], wherein the local controller plays the role of the slave. The centralized master-level controller broadcasts the global status of the PV sources and reduces fluctuations in the system. Similarly, the robustness in the presence of disturbances and stability due to TD of DCMG is studied in MAS [12]. The uncertainty in the energy internet with TD is investigated in the [40].

Distributed cooperative is an effective method for achieving global consensus, however, this method can result as poor voltage regulation especially when line impedances are significant [41]–[43]. This problem can be somehow tackled by considering a second level centralized controller that would provide the voltage restoration term. MAS-based distributed system is one of the new methods. Where MAS-based secondary voltage cooperative control strategy is applied to achieve the global bus voltage. The MAS-based control system in [12], [19] have considered only radial system. The authors in [38] have considered dc-ring system with two-level MAS-based controller; however, the delay between the first and second level agents are neglected. The disadvantage of MAS-based systems is the need of scattered communication network. In the master-slave based control the delay considered is only between the master and the slave controllers and no delay is consideration among the DGUs.

In the control systems, the TD compensation problem using linear-matrix-inequality (LMI) can be classified into two categories [44], [45]: 1) delay-independent stabilization and 2) delay-dependent stabilization. The stabilization of the delay-independent approach is more conservative in general in comparison with that of the delay-dependent approach. The communication delay in the DC ImG understudy is within the range of several hundred milliseconds [35]; therefore, the delay-dependent stabilization approach is a more appropriate strategy.

In this study, we attempted to investigate the effects of the communication delays in the DC ImG and propose centralized control schemes. The objective of the controller is to effectively control voltage, stabilize, reduce or reject disturbance of DC ImG. To propose such controller, we investigate three controllers: simple stabilizing, robust H_∞, and predictor based robust H_∞ controllers using the delay-dependent stabilization approach.

This study aims to analyze the effect of the TD on the stability of DC ImG and propose centralized controller strategies to attain voltage stability in a DC ImG under communication link delay. The significant contributions made by this study are as follows:

(i) Although, many authours have provided the time-delay-system (TDS) modeling of DC ImG, however, in this study we are providing the TDS modeling of the DC ImG for centralized controller. The system includes disturbances along with the communication link delay. Further, the stability analysis of DC ImG under TD is performed; the LMI constraints are derived for stability that would also ensure the robustness fo the system. As an insight, the stability of TDS is assured by Lyapunov-Krasovskii functionals (LKFs), whereas the robustness is achieved through $\mathcal{L}_2$-norm minimization.

(ii) To the best of the authors' knowledge, the prediction-based memory control of DC ImG with disturbance and time-delay is performed for the frist time.

(iii) In addition to the prediction-based controller stabilizing and robust controllers are also implemented to compare the performance of the proposed controller.

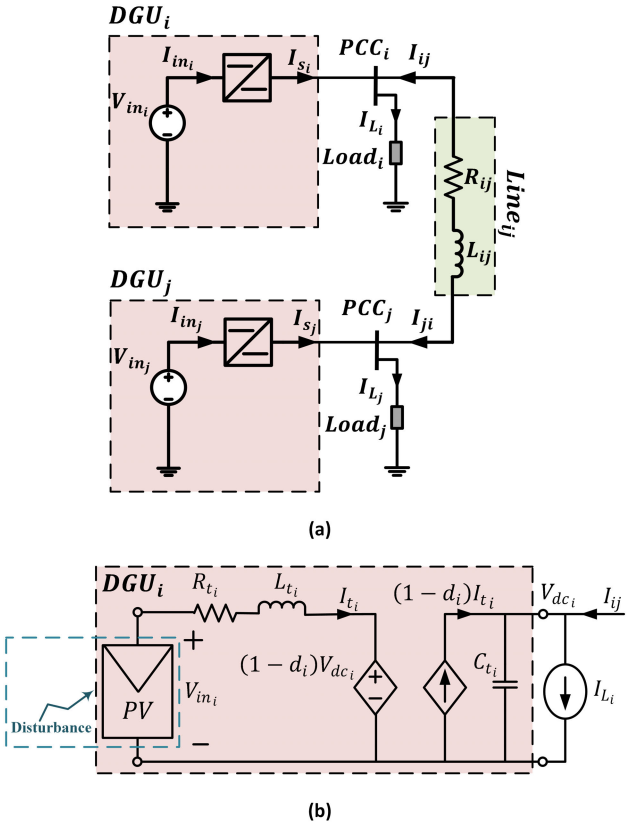

FIGURE 1. (a) Coupled DGUs; (b) average model of DGU_i.

The rest of this paper is organized as follows. Section II presents the state-space dynamics of the DC ImG. The error and TD dynamics of DC ImG are also discussed in this section. The effects of communication delay in DC ImG on its stability and control are also investigated in Section III. The simulation results and its discussion are presented in Section IV. Finally, Section V concludes this research.

Some notations considered in this paper are as follows: Identity matrix is denoted by I, where for zero matrices, '0' is used. The matrix $A^\top$ denotes the transpose of matrix A. An asterisk $(*)$ sign is used to represent transposed off-diagonal elements of symmetric matrices. The positive-definite and positive semi-definite matrices are denoted as $P > 0$ and $P \geq 0$, respectively. Similarly, the expressions $P < 0$ and $P \leq 0$ mean negative-definite and negative semi-definite matrices, respectively. The mathematical lemmas and theorems applied are discussed in the paper.

II. DYNAMIC MODELING OF DC IMG

In this section, we present the dynamic model of the DC ImG. To develop the model, we first consider the simple case of coupled DC ImG with no communication and control delay, as illustrated in Fig. 1(a). The coupled DGU case is then extended to N-DGUs. In the second part, we present the dynamical representation of the DC ImG with communication delay.

A. DC IMG WITH NO COMMUNICATION DELAY

For the coupled-DGU case, consider DGU_i and DGU_j in Fig. 1(a). The DGUs are coupled via a line $Line_{ij}$ at the point-of-common-coupling (PCC). The coupling line has a resistive part R_{ij} and an inductive component L_{ij}. The connected DGU can be any DC-DC type converter (e.g., buck or boost). In this study, the boost-type converter is considered, and its average model is depicted in Fig. 1(b). In the average model, V_{in} represents a generic input DC voltage source, which is typically a renewable source (e.g., solar PV). The loads $Load_i$ and $Load_j$ in the coupled-DGU system are unknown. Therefore, they are modeled as current disturbances I_{L_i}. Additionally, let the large-signals of DGU_i be $\Sigma = \{V_{dc_i}, V_{in_i}, I_{L_i}, I_{t_i}, d_i\}$ [7], [25], [26]. Furthermore, let $\sigma \in \Sigma$ be the sum $\sigma = \bar{\sigma} + \tilde{\sigma}$, such that $\bar{\sigma}$ is a DC quiescent value, and $\tilde{\sigma}$ is the small AC signal superimposed over the DC value [46]. Then, the small-signal dynamical model of DGU_i can be expressed as follows:

$$DGU_i := \begin{cases} \dot{\tilde{x}}_i(t) = A_{ii}\tilde{x}_i(t) + B_i\tilde{u}_i(t) \\ \qquad\qquad +D_i\tilde{w}_i(t) + \tilde{\zeta}_i(t) \\ \tilde{y}_i(t) = C_i\tilde{x}_i(t) \end{cases} \tag{1}$$

where $\tilde{x}_i(t) = [\tilde{v}_{dc_i}, \tilde{i}_{dc_i}]^\top$ is the small-signal state vector, $\tilde{u}_i(t) = \tilde{d}_i(t)$ is the small-signal pulse width modulation (PWM) input, $\tilde{w}_i(t) = [\tilde{i}_{L_i}, \tilde{v}_{in_i}]^\top$ is the small-signal exogenous disturbance vector, $\zeta_i(t) = A_{ij}\tilde{x}_j$ is the coupling term between both DGUs, and $\tilde{y}_i(t)$ is the output vector. $A_{ij} = diag(\frac{1}{R_{ij}C_{t_i}}, 0)$, $D_i = diag(\frac{-1}{C_{t_i}}, \frac{1}{L_{t_i}})$, $C_i = I_{2\times 2}$, $A_{ii} = \begin{bmatrix} \frac{-1}{R_{ij}C_{t_i}} & \frac{(1-\bar{D}_i)}{C_{t_i}} \\ \frac{-(1-\bar{D}_i)}{L_{t_i}} & \frac{-R_{t_i}}{L_{t_i}} \end{bmatrix}$, and $B_i = \begin{bmatrix} \frac{-\bar{I}_{t_i}}{C_{t_i}} \\ \frac{\bar{V}_{dc_i}}{L_{t_i}} \end{bmatrix}$.

In the system (1), the quasi-stationary line (QSL) approximation in [13] has been considered. The small-signal dynamical equation of DGU_j in Fig. 1(a) is similar to the equation of DGU_i.

Now, for the system (1), let the small-signal dynamic of the error be expressed by the difference between the reference and output voltages as (3) follows:

$$\dot{\tilde{e}}_i = -h_i(V_{ref_i} - V_{dc_i}) = -h_i\tilde{v}_{dc_i}, \tag{2}$$

where h_i is the free design parameter of the error dynamics. Hence, the small-signal augmented system of (1) is

$$D\hat{G}U_i := \begin{cases} \dot{\hat{x}}_i(t) = \hat{A}_{ii}\hat{x}_i(t) + \hat{B}_i\hat{u}_i(t) \\ \qquad\qquad +\hat{D}_i\hat{w}_i(t) + \hat{\zeta}_i(t) \\ \hat{y}_i(t) = \hat{C}_i\hat{x}_i(t), \end{cases} \tag{3}$$

where $\hat{x}_i(t) = [\tilde{v}_{dc_i}, \tilde{i}_{dc_i}, \tilde{e}_i]^\top$ is the augmented state vector, $\hat{u}_i(t) = \tilde{d}_i(t)$ is a PWM control, $\hat{w}_i(t) = [\tilde{i}_{L_i}, \tilde{v}_{in_i}]^\top$ represents the disturbances, $\hat{\zeta}_i = [\tilde{\zeta}_i^\top(t), 0^\top]^\top$ is the coupling term, and $\hat{y}_i(t) = [\tilde{v}_{dc_i}, \tilde{i}_{dc_i}, \tilde{e}_i]^\top$ is the augmented output vector. $\hat{C}_i = I_{3\times 3}$, $H_i = [h_i, 0]$, $\hat{A}_{ii} = \begin{bmatrix} A_{ii} & \mathbf{0} \\ -H_iC_i & \mathbf{0} \end{bmatrix}$, $\hat{B}_i = \begin{bmatrix} B_i \\ \mathbf{0} \end{bmatrix}$, and $\hat{D}_i = \begin{bmatrix} D_i \\ \mathbf{0} \end{bmatrix}$.

The augmented small-signal dynamical system representation of $D\hat{G}U_j$ is similar to (3). Therefore, the coupled DGU equation of Fig. 1(a) can be expressed as follows:

$$\begin{cases} \dot{\hat{\mathbf{x}}}(t) = \hat{\mathbf{A}}\hat{\mathbf{x}}(t) + \hat{\mathbf{B}}\hat{\mathbf{u}}(t) + \hat{\mathbf{D}}\hat{\mathbf{w}}(t) \\ \hat{\mathbf{y}}(t) = \hat{\mathbf{C}}\hat{\mathbf{x}}(t), \end{cases} \tag{4}$$

where $\hat{\mathbf{x}} = [\hat{x}_i, \hat{x}_j]^\top$, $\hat{\mathbf{u}} = [\hat{u}_i, \hat{u}_j]^\top$, $\hat{\mathbf{w}} = [\hat{w}_i, \hat{w}_j]^\top$, $\hat{\mathbf{y}} = [\hat{y}_i, \hat{y}_j]^\top$, $\hat{\mathbf{B}} = diag\ (\hat{B}_i, \hat{B}_j)$, $\hat{\mathbf{D}} = diag\ (\hat{D}_i, \hat{D}_j)$, $\hat{\mathbf{C}} = diag\ (\hat{C}_i, \hat{C}_j)$, $\hat{A}_{ij} = diag(A_{ij}, \mathbf{0})$, and $\hat{\mathbf{A}} = \begin{bmatrix} \hat{A}_{ii} & \hat{A}_{ij} \\ \hat{A}_{ji} & \hat{A}_{jj} \end{bmatrix}$.

Similarly, for the DC ImG with N DGUs, let $\mathcal{D} = \{1, \ldots, \mathcal{N}\}$, $\mathcal{N}_i \subset \mathcal{D}$ and DGU_i be coupled via links $Line_{ij}$ to neighboring $DGUs$. The vectors and matrices in (4) become the length and dimensions of N as follows: $\hat{\mathbf{x}} = [\hat{x}_1, \hat{x}_2, \ldots, \hat{x}_N]^\top$, $\hat{\mathbf{u}} = [\hat{u}_1, \hat{u}_2, \ldots, \hat{u}_N]^\top$, $\hat{\mathbf{w}} = [\hat{w}_1, \hat{w}_2, \ldots, \hat{w}_N]^\top$, $\hat{\mathbf{y}} = [\hat{y}_1, \hat{y}_2, \ldots, \hat{y}_N]^\top$, $\hat{\mathbf{B}} = diag\ (\hat{B}_i)$, $\hat{\mathbf{C}} = diag\ (\hat{C}_i)$, $\hat{\mathbf{D}} = diag\ (\hat{D}_i)$, $\hat{\zeta}_i(t) = \sum_{j\in\mathcal{N}_i} \hat{A}_{ij}\hat{x}_j(t)$,

$$\hat{\mathbf{A}} = \begin{bmatrix} \hat{A}_{11} & \hat{A}_{12} & \ldots & \hat{A}_{1N} \\ \hat{A}_{21} & \hat{A}_{22} & \ldots & \hat{A}_{2N} \\ \vdots & \vdots & \ddots & \vdots \\ \hat{A}_{N1} & \hat{A}_{N2} & \ldots & \hat{A}_{NN} \end{bmatrix}, \hat{A}_{ij} = diag(A_{ij}, \mathbf{0}), \text{ and}$$

$$\hat{A}_{ii} = \begin{bmatrix} \frac{1}{C_{t_i}} \sum_{j\in\mathcal{N}_i} \frac{-1}{R_{ij}} & \frac{(1-\bar{D}_i)}{C_{t_i}} & 0 \\ \frac{-(1-\bar{D}_i)}{L_{t_i}} & \frac{-R_{t_i}}{L_{t_i}} & 0 \\ h_i & 0 & 0 \end{bmatrix}.$$

B. TIME-DELAY IN DC IMG

In this section, we discuss the fundamental dynamical model of the TDS for the DC ImG illustrated in Fig. 2. Assume that the overall time-delay of the system is τ, which is composed of the delay in the communication network, sensors' measurements, and feedback path delay. Considering the presence of time-delay in the control-input, the dynamical system in (4) becomes

$$\begin{cases} \dot{\hat{\mathbf{x}}}(t) = \hat{\mathbf{A}}\hat{\mathbf{x}}(t) + \hat{\mathbf{B}}\hat{\mathbf{u}}(t - \tau/2) + \hat{\mathbf{D}}\hat{\mathbf{w}}(t) \\ \hat{\mathbf{y}}(t) = \hat{\mathbf{C}}\hat{\mathbf{x}}(t), \end{cases} \tag{5}$$

where $\hat{\mathbf{u}}(t - \tau/2) = [\hat{u}_1(t - \tau/2), \hat{u}_2(t - \tau/2), \ldots, \hat{u}_N(t - \tau/2)]^\top$, $\tau \in [0, h]$ is the delay, and the other parameters are similar to the system (4). In the next section, the TD-system in (5) is used to analyze and develop TDS controllers.

III. TIME-DELAY CONTROL IN DC IMG

In this section, we present the proposed controllers for the TDS (5). Consider the state-feedback $\hat{\mathbf{u}}(t) = \mathbf{K}\hat{\mathbf{x}}(t - \tau/2)$. Then, the half time-delay $\tau/2$ for $\hat{\mathbf{u}}(t)$ (as depicted in Fig. 2) can be expressed as

$$\hat{\mathbf{u}}(t - \tau/2) = \mathbf{K}\hat{\mathbf{x}}(t - \tau) \tag{6}$$

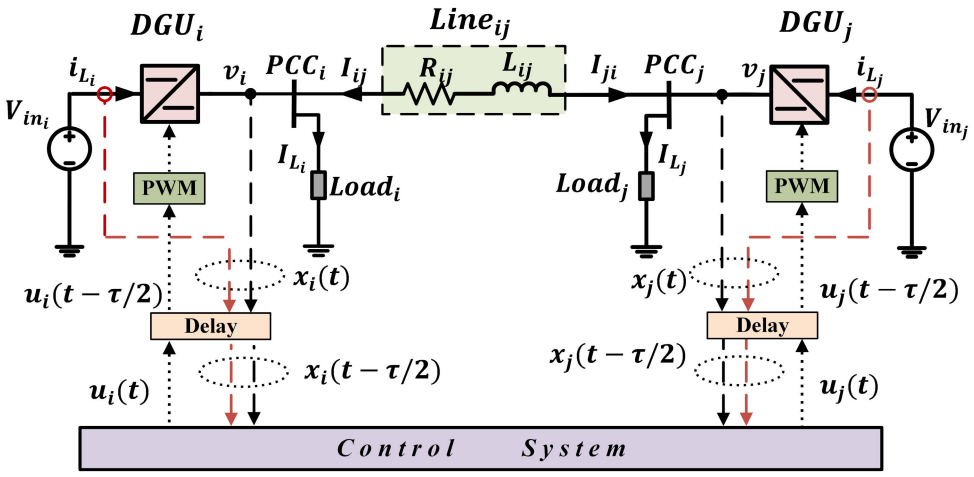

FIGURE 2. Schematic of coupled DGUs with communication delay $\tau \in [0, h]$.

Substituting (6) in the TDS (5) results in the following closed-loop system

$$\begin{cases} \dot{\hat{\mathbf{x}}} = \hat{\mathbf{A}}\hat{\mathbf{x}}(t) + \hat{\mathbf{B}}\mathbf{K}\hat{\mathbf{x}}(t-\tau) + \hat{\mathbf{D}}\hat{\hat{\mathbf{w}}}(t) \\ \hat{\mathbf{y}}(t) = \hat{\mathbf{C}}\hat{\mathbf{x}}(t), \end{cases} \tag{7}$$

where $\hat{\mathbf{x}}(t-\tau) = [\hat{x}_1(t-\tau), \hat{x}_2(t-\tau), \ldots, \hat{x}_N(t-\tau)]^\top$, and the other parameters of (7) are similar to the system (4).

For the stable operation of the system (5), we need to determine the gain $\mathbf{K}$, such that the closed-loop system (7) is asymptotically stable. In the next sub-sections, we investigate and propose three TDS controllers.

A. STABILIZING CONTROLLER

Our objective with respect to the stabilizing controller is to determine a state-feedback gain (6) that asymptotically stabilizes the closed-loop system (7). The stabilizing controller is illustrated in Fig. 3(a), which can be obtained by the following theorem.

Theorem 1: The state-feedback gain $\mathbf{K}_s$ stabilizes the closed-loop system (7) asymptotically if there exist matrices $\bar{\mathbf{P}} > \mathbf{0}$, $\bar{\mathbf{S}} \geq \mathbf{0}$, $\bar{\mathbf{R}} \geq \mathbf{0}$, and $\bar{\mathbf{Q}} \geq \mathbf{0}$ with scalars $d > 0$ and $\epsilon > 0$, such that the following LMIs are guaranteed:

$$\bar{\Phi} = \begin{bmatrix} \bar{\phi}_{11} & \bar{\phi}_{12} & \bar{\mathbf{S}}_{12} & \bar{\phi}_{14} \\ * & \bar{\phi}_{22} & \mathbf{0} & \epsilon\hat{\mathbf{B}}\mathbf{Y} \\ * & * & -(\bar{\mathbf{S}}+\bar{\mathbf{R}}) & \bar{\mathbf{R}} - \bar{\mathbf{S}}_{12}^\top \\ * & * & * & \bar{\phi}_{44} \end{bmatrix} < \mathbf{0} \tag{8}$$

$$\begin{bmatrix} \bar{\mathbf{R}} & \bar{\mathbf{S}}_{12} \\ * & \bar{\mathbf{R}} \end{bmatrix} \geq \mathbf{0}, \tag{9}$$

where $\bar{\phi}_{11} = \hat{\mathbf{A}}\bar{P}_2 + \bar{\mathbf{P}}_2^\top\hat{\mathbf{A}}^\top + \bar{\mathbf{S}} + \bar{\mathbf{Q}} - \bar{\mathbf{R}}$,
$\bar{\phi}_{12} = \bar{\mathbf{P}} - \bar{\mathbf{P}}_2 + \epsilon\bar{\mathbf{P}}_2^\top\hat{\mathbf{A}}^\top$, $\bar{\phi}_{14} = \hat{\mathbf{B}}\mathbf{Y} + \bar{\mathbf{R}} - \bar{\mathbf{S}}_{12}$,
$\bar{\phi}_{22} = -\epsilon\bar{\mathbf{P}}_2 - \epsilon\bar{\mathbf{P}}_2^\top + h^2\bar{\mathbf{R}}$,
$\bar{\phi}_{44} = -(1-d)\bar{\mathbf{Q}} - 2\bar{\mathbf{R}} + \bar{\mathbf{S}}_{12} + \bar{\mathbf{S}}_{12}^\top$, $\bar{\mathbf{P}}_2 = \mathbf{P}_2^{-1}$.

The controller gain is obtained by $\mathbf{K}_s = \mathbf{Y}\bar{\mathbf{P}}_2^{-1}$.

Proof 1: The proof of Theorem 1 is presented in Appendix A.

B. ROBUST CONTROLLER

Consider the QSL-ImG model in (5) as an MIMO time-delay system.

$$\begin{cases} \dot{\hat{\mathbf{x}}}(t) = \hat{\mathbf{A}}\hat{\mathbf{x}}(t) + \hat{\mathbf{B}}\hat{\mathbf{u}}(t-\tau/2) + \hat{\mathbf{D}}\hat{\mathbf{w}}(t) \\ \hat{\mathbf{z}}(t) = \hat{\mathbf{C}}_1\hat{\mathbf{x}}(t) + \hat{\mathbf{D}}_{11}\hat{\mathbf{w}}(t) + \hat{\mathbf{D}}_{12}\hat{\mathbf{u}}(t-\tau/2) \\ \hat{\mathbf{y}}(t) = \hat{\mathbf{C}}_2\hat{\mathbf{x}}(t) + \hat{\mathbf{D}}_{21}\hat{\mathbf{w}}(t) + \hat{\mathbf{D}}_{22}\hat{\mathbf{u}}(t-\tau/2), \end{cases} \tag{10}$$

where $\hat{\mathbf{x}}(t)$ is the state vector; $\hat{\mathbf{u}}(t-\tau/2)$ is the TD control input; $\hat{\mathbf{w}}(t)$ is the exogenous disturbance; $\hat{\mathbf{z}}(t)$ represents the controlled output; and $\hat{\mathbf{y}}(t)$ is the measured output. The measuring noise matrix $\hat{\mathbf{D}}_{21} = \mathbf{0}$, and feed-through matrix $\hat{\mathbf{D}}_{22} = \mathbf{0}$, because no measurement noise and direct feed-through from the control input to the output exists. Furthermore, the disturbance is zero in the controlled output; thus, $\hat{\mathbf{D}}_{11} = \mathbf{0}$. The dimensions of the other matrices when the system comprises N *DGUs* of the non-zero matrices are $\hat{\mathbf{A}} \in \mathbb{R}^{3N\times 3N}$, $\hat{\mathbf{B}} \in \mathbb{R}^{3N\times N}$, $\hat{\mathbf{C}}_1 \in \mathbb{R}^{4N\times 3N}$, $\hat{\mathbf{C}}_2 \in \mathbb{R}^{3N\times 3N}$, $\hat{\mathbf{D}} \in \mathbb{R}^{3N\times 2N}$, and $\hat{\mathbf{D}}_{12} \in \mathbb{R}^{4N\times N}$.

For a robust controller, we seek a state-feedback gain $\mathbf{K}_\infty$ that internally stabilizes the TDS DC ImG (10) and leads to $\mathcal{L}_2$-gain of the system less than γ. The control input can be expressed as follows:

$$\hat{\mathbf{u}}(t-\tau/2) = \mathbf{K}_\infty\hat{\mathbf{x}}(t-\tau) \tag{11}$$

This robust controller is obtained by theorem 2, and the closed-loop system is depicted in Fig. 3(b) and is mathematically expressed as follows:

$$\begin{cases} \dot{\hat{\mathbf{x}}}(t) = \hat{\mathbf{A}}\hat{\mathbf{x}}(t) + \hat{\mathbf{B}}\mathbf{K}_\infty\hat{\mathbf{x}}(t-\tau) + \hat{\mathbf{D}}\hat{\mathbf{w}}(t) \\ \hat{\mathbf{z}}(t) = \hat{\mathbf{C}}_1\hat{\mathbf{x}}(t) + \hat{\mathbf{D}}_{12}\mathbf{K}_\infty\hat{\mathbf{x}}(t-\tau) \\ \hat{\mathbf{y}}(t) = \hat{\mathbf{C}}_2\hat{\mathbf{x}}(t) \end{cases} \tag{12}$$

Theorem 2: For the TDS (10), a robust state-feedback controller with gain $\mathbf{K}_\infty$ (11) asymptotically stabilizes the system (12) without disturbances. Additionally, under zero

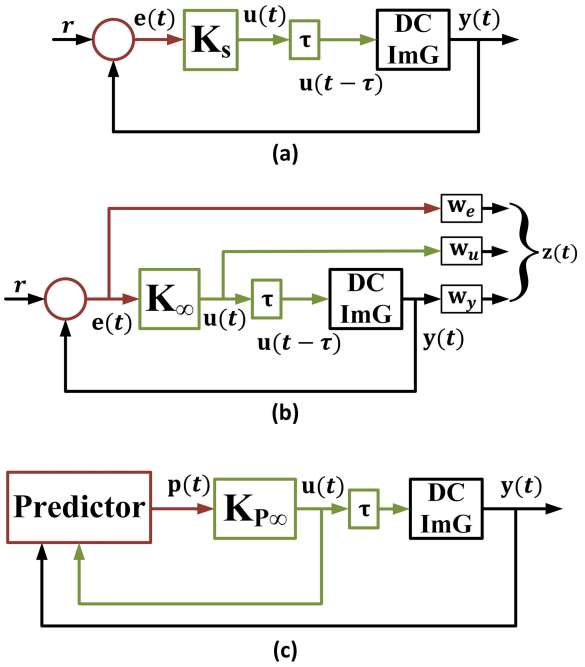

FIGURE 3. Proposed TDS controllers: (a) stabilizing controller theorem 1, (b) robust controller theorem 2, (c) predictor-based controller theorem 3.

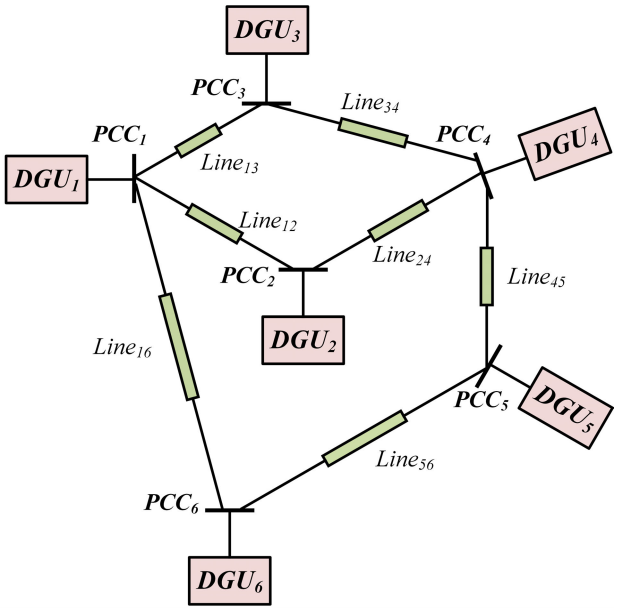

FIGURE 4. DC ImG consisting of six *DGUs*.

initial condition $\hat{\mathbf{x}}(0) = \mathbf{0}$, $\forall\ \hat{\mathbf{w}} \in \mathcal{L}_2\ [0, \infty)$, the closed-loop system guarantees inequality $\|\hat{\mathbf{z}}\|_{\mathcal{L}_2}^2 \leq \gamma^2 \|\hat{\mathbf{w}}\|_{\mathcal{L}_2}^2$, and LMI (9) holds, where $\gamma > 0$ is a prescribed scalar.

$$\phi = \left[\begin{array}{c|cc} \bar{\Phi} & \hat{\mathbf{D}} & \bar{\mathbf{P}}_2^\top \hat{\mathbf{C}}_1^\top \\ & \epsilon\hat{\mathbf{D}} & \mathbf{0} \\ & \mathbf{0} & \mathbf{0} \\ & \mathbf{0} & \mathbf{Y}^\top \hat{\mathbf{D}}_{12}^\top \\ \hline * & -\gamma\mathbf{I} & \mathbf{0} \\ & * & -\mathbf{I} \end{array}\right] < 0 \tag{13}$$

Proof 2: The proof of Theorem 2 is presented in Appendix B.

C. PREDICTOR-FEEDBACK BASED ROBUST CONTROLLER

In this section, we propose a memory-based state-feedback robust H_∞ controller for the TDS (10). In the first step, the prediction vector for the system is determined. Then, the predictor vector is used in the control input.

For the system (10), let $\hat{\mathbf{u}}(t) = \phi_u(t)$ with $\tau = h > 0$ constant delay. Furthermore, let $\phi_u(t)$ be a real-valued initial function on interval $t \in [-h,\ 0]$. Moreover, we assume that the exogenous disturbance $\hat{\mathbf{w}}(t)$ is square-integrable, [47], i.e.,

$$||\hat{\mathbf{w}}(t)||_{\mathcal{L}_2}^2 = \int_0^\infty ||\hat{\mathbf{w}}(s)||^2 ds < M.$$

We are interested in the robust stability of the system (10), such that the systems without exogenous disturbances become asymptotically stable. Furthermore, the impact of the disturbances on the system performance is minimized. This objective is similar to the robust controller in Theorem 2. However, the only difference between the predictor-based robust controller and the robust-controller (Theorem 2) is that the effect of the time-delay in the input is compensated by the predictor feedback. Hence, the prediction vector for the system is constructed for the control input.

Lemma 1 [48] : For constant matrix $M \in \mathbb{R}^{m\times m}$, $M = M^\top > 0$, vector function $\omega : [0\quad \varphi] \to \mathbb{R}^m$, and scalar $\varphi > 0$, such that the integration below is defined

$$\varphi \int_0^\varphi \omega^\top(\beta) M \omega(\beta) d\beta \geq \left[\int_0^\varphi \omega(\beta) d\beta\right]^\top M \left[\int_0^\varphi \omega(\beta) d\beta\right]$$

Lemma 2 [47]: The prediction vector for TD system (10) with $h = \tau$ is given by

$$\begin{aligned} \bar{\mathbf{p}}(t) &= \hat{\mathbf{x}}(t+\tau) \\ &= e^{\hat{\mathbf{A}}\tau}\hat{\mathbf{x}}(t) + \int_{t-\tau}^{t} e^{\hat{\mathbf{A}}(t-s)}[\hat{\mathbf{B}}\hat{\mathbf{u}}(s) + \hat{\mathbf{D}}\hat{\mathbf{w}}(s+\tau)]ds \end{aligned} \tag{14}$$

Lemma 3: For $\hat{\mathbf{w}} = 0$ (i.e., absence of exogenous disturbances), the prediction vector (14) for $h = \tau$ is given by

$$\begin{aligned} \mathbf{p}(t) &= \hat{\mathbf{x}}(t+\tau) - \int_{t-\tau}^{t} e^{\hat{\mathbf{A}}(t-s)}[\hat{\mathbf{D}}\hat{\mathbf{w}}(s+\tau)]ds \\ &= e^{\hat{\mathbf{A}}\tau}\hat{\mathbf{x}}(t) + \int_{t-\tau}^{t} e^{\hat{\mathbf{A}}(t-s)}[\hat{\mathbf{B}}\hat{\mathbf{u}}(s)]ds \end{aligned} \tag{15}$$

From (14) and (15), we can write $\bar{\mathbf{p}}(t) = \mathbf{p}(t) + \hat{\mathbf{e}}_p(t)$, where

$$\hat{\mathbf{e}}_p(t) = \int_{t-s}^{t} e^{\hat{\mathbf{A}}(t-s)}[\hat{\mathbf{D}}\hat{\mathbf{w}}(s+\tau)]ds \tag{16}$$

At this stage, we can formulate the prediction-based controller with the following structure:

$$\hat{\mathbf{u}}(t) = \mathbf{K}_{P\infty}\mathbf{p}(t) = \mathbf{K}_{P\infty}\bar{\mathbf{p}}(t) - \mathbf{K}_{P\infty}\hat{\mathbf{e}}_p(t) \tag{17}$$

TABLE 1. System parameters of the DC ImG Fig. 4.

Parameter	Description	Unit	DGU_1	DGU_2	DGU_3	DGU_4	DGU_5	DGU_6
V_{ref_i}	Reference voltage	V	381.0	380.5	380.2	379.0	379.5	380.7
V_{in_i}	Input voltage	V	95	100	90	105	92	90
$\bar{D}_i$	Duty cycle	-	0.751	0.737	0.763	0.723	0.757	0.764
$Load_i$	DGU load	kW	2.5	2.0	1.8	2.5	3.0	2.5
C_{t_i}	Capacitance	μF	172.3	169.7	176.0	167.9	175.3	175.6
L_{t_i}	Inductance	μH	243.9	265.4	222.5	286.9	230.8	222.7
R_{t_i}	Resistance	Ω	0.02	0.04	0.02	0.2	0.4	0.5
R_{ij}	Line resistance	Ω	0.5-2-10	0.5-4	2-4	4-4-15	15-4	10-4
L_{ij}	Line inductance	μH	10-70-800	10-70	70-70	70-70-25	25-90	800-90
Switching frequency $(f_{sw}) = 25kHz$.								

TABLE 2. Values for the parameters used in Theorems 1, 2 and 3, $i \in [1, 6]$.

Controllers	Parameter	Delay (τ) in ms		
		5	10	20
Stabilizing	d	0.1	0.1	0.1
	ϵ	10^{-4}	10^{-4}	10^{-4}
	h_i	10^3	10^3	10^3
Robust	d	0.1	0.1	0.1
	ϵ	10^{-4}	10^{-4}	10^{-4}
	γ	14	556	2206
Predictor	β	2	2	2
	$\bar{\mathbf{u}}$	1	1	1
	λ	1	1	1
	γ	55	55	55
Robust and Predictor	h_i	10^3	10^3	10^3
	w_{v_i}	0.6	0.6	0.6
	w_{i_i}	0.1	0.1	0.1
	w_{e_i}	0.2	0.2	0.2
	w_{u_i}	1	1	1

From Lemma 2, we can write the delayed input of the predictor-based control system as

$$\hat{\mathbf{u}}(t-\tau) = \mathbf{K}_{P\infty}\hat{\mathbf{x}}(t) - \mathbf{K}_{P\infty}\hat{\mathbf{e}}_p(t-\tau) \tag{18}$$

In the TDS (10), the delay is $\tau/2$, whereas in the predictor-based control input (18), it is τ, although the state itself is not available in the central controller (it is received with $\tau/2$ delay), and this forward delay (from DGU to controller) is compensated with the return delay $\tau/2$ (from central controller to DGU). Substituting (18) in the TDS (10), the closed-loop system becomes

$$\begin{cases} \dot{\hat{\mathbf{x}}}(t) = (\hat{\mathbf{A}} + \hat{\mathbf{B}}\mathbf{K}_{P\infty})\hat{\mathbf{x}}(t) + \mathbf{D}_1\bar{\mathbf{w}}(t) \\ \hat{\mathbf{z}}(t) = (\hat{\mathbf{C}}_2 + \hat{\mathbf{D}}_{12}\mathbf{K}_{P\infty})\hat{\mathbf{x}}(t) + \bar{\mathbf{D}}_{\mathbf{12}}\bar{\mathbf{w}}(t) \end{cases} \tag{19}$$

where $\mathbf{D}_1 = [\hat{\mathbf{D}} \;\; \hat{\mathbf{B}}]$, $\bar{\mathbf{w}} = [\hat{\mathbf{w}}^\top \;\; \tilde{\mathbf{w}}^\top]^\top$, $\tilde{\mathbf{w}} = -\mathbf{K}_{P\infty}\hat{\mathbf{e}}_p(t-\tau)$, and $\bar{\mathbf{D}}_{\mathbf{12}} = [\mathbf{0} \;\; \hat{\mathbf{D}}_{12}]$.

In the closed-loop system (19), $\bar{\mathbf{w}}$ represents the new disturbance vector, and for robustness, its effect on the DC ImG should be minimized according to $\mathcal{L}_2$-norm reduction criterion. Moreover, this disturbance must also be square integrable, which is discussed in the Lemma 4. The block diagram representation of the prediction-based robust controller is depicted in Fig. 3(c).

Lemma 4 [47]: If the external disturbance vector $\hat{\mathbf{w}}$ of TDS (10) is square integrable, then the new disturbance vector $\bar{\mathbf{w}}$ is also square integrable.

TABLE 3. Feasibility of LMIs for different communication delays.

Controller	Delay τ in (ms)				
	5	10	20	50	100
Stabilizing	FB	FB	FB	FB	FB
Robust	FB	FB	FB	N.FB	N.FB
Predictor	FB	FB	FB	FB	FB

FB: Feasible. N.FB: Not feasible.

TABLE 4. Controllers gains $\mathbf{K}_s$, $\mathbf{K}_\infty$, and $\mathbf{K}_{P\infty}$ for stabilizing, robust, and prediction-based controllers respectively.

K	Gain for $20ms$ delay
$\mathbf{K}_s$	-6.8e-5, 5.9e-6, 2.0e-7, 4.3e-5, -4.9e-8, -2.6e-8, 1.3e-5, -1.3e-6, -2.3e-8, 1.2e-5, -3.9e-6, -1.1e-8, 7.6e-7, -2.8e-6, 2.3e-9, -1.6e-6, -3.2e-7, 2.5e-8 6.3e-5, -1.2e-6, -8.0e-8, -7.6e-5, 6.8e-6, 2.5e-7, 1.3e-6, -1.7e-6, -1.9e-8, 1.2e-5, -2.6e-6, 1.3e-8, -1.7e-6, 5.5e-7, -4.5e-9, 1.6e-6, -6.0e-7, -1.2e-8 5.4e-6, -6.2e-7, -2.5e-8, 6.2e-6, -1.5e-6, -1.5e-8, -2.1e-5, 4.6e-6, 1.7e-7, 1.1e-5, -2.4e-6, 8.2e-9, 3.4e-7, -1.1e-6, -2.2e-9, -1.6e-6, -1.4e-7, -5.2e-9 1.1e-5, -4.4e-6, -2.0e-8, 1.6e-5, -4.3e-6, -4.6e-8, 9.1e-6, -2.0e-6, -6.2e-8, -3.7e-5, 1.1e-5, 2.7e-7, -5.9e-6, 1.4e-6, 1.5e-8, -4.5e-7, -4.8e-6, 2.3e-9 -9.9e-8, 2.5e-7, -2.8e-8, -5.1e-6, 3.8e-7, -1.2e-8, -1.6e-6, -2.8e-7, -6.6e-9, 7.5e-6, -1.8e-6, -2.7e-8, 3.3e-6, 8.1e-6, 2.2e-7, -2.4e-6, 4.7e-6, 8.1e-11 8.0e-6, -9.7e-7, -4.8e-8, -4.2e-6, -3.1e-7, -8.9e-9, 1.9e-6, -7.5e-7, -4.3e-9, -7.3e-6, 7.8e-7, -9.1e-9, -3.4e-6, 6.0e-6, -4.1e-8, 8.5e-6, 9.1e-6, 2.1e-7
$\mathbf{K}_\infty$	-1.6e-8, -3.2e-7, 6.1e-7, -3.0e-9, 2.5e-9, -2.2e-7, -3.7e-10, 2.4e-10, -5.4e-8, 8.4e-10, -4.1e-10, -8.9e-11, -4.5e-10, 1.7e-9, 1.2e-10, 3.3e-9, 2.1e-9, -1.2e-8 -4.6e-10, -1.7e-9, -4.1e-7, -2.7e-8, -3.6e-7, 8.1e-7, -6.8e-10, -1.2e-9, 2e-9, -6.6e-9, 2.9e-9, -5e-8, 5.5e-10, -1.1e-9, 4.4e-10, -3.4e-9, -2.0e-9, 1.3e-9 2.6e-10, -4.8e-10, -5.7e-8, 2.7e-10, -6.7e-10, 1.1e-9, -1.8e-8, -3e-7, 4e-7, -1.7e-9, 1.5e-9, -2.8e-8, 1.7e-10, -1.3e-10, 9.2e-11, -6.8e-10, -3.3e-10, 1.8e-10 -6.1e-9, 1.6e-9, 9.6e-10, -7.2e-9, 1.5e-9, -2.5e-7, -2.0e-9, -8.2e-10, -2.5e-7, -1.5e-7, -4.1e-7, 9.6e-7, -2.7e-9, 8.5e-10, -6.8e-8, 2.1e-9, 1.8e-9, 6.2e-10 -5.7e-10, 1.0e-9, 1.5e-9, -6.7e-11, 9.9e-10, -3.4e-10, -8.8e-10, 1.4e-9, -1.5e-10, 1.5e-9, 1.7e-9, -1.7e-7, -4.5e-7, -3.6e-7, 1.2e-6, 7.7e-9, -8.8e-10, -6.5e-7 3.0e-9, -6.4e-10, -3.3e-7, 2.7e-9, -1.2e-9, 1.2e-9, 4.2e-10, -1.1e-10, 1.3e-10, -4.9e-9, 1.1e-9, 1.3e-9, 1.1e-8, -6.2e-10, -8.4e-7, -6.0e-7, -3.6e-7, 1.5e-6
$\mathbf{K}_{P\infty}$	-4.5e-3, -4.5e-3, 7.9e-3, -2.6e-3, -8.5e-4, -2.5e-3, -2.1e-3, -4.3e-4, -1.1e-3, -1.4e-3, -5.5e-4, -2.2e-4, -2.6e-4, -7.8e-6, -4.6e-5, -6.9e-4, -1.2e-4, -1.0e-4 -3.3e-3, -7.2e-4, -1.9e-3, -5.4e-3, -4.4e-3, 7.7e-3, -2.2e-3, -3.6e-4, -5.6e-4, -1.8e-3, -5.8e-4, -3.4e-4, -2.0e-4, 1.8e-5, -3.1e-5, -5.7e-4, -7.9e-5, -4.5e-6 -2.2e-3, -5.8e-4, -9.3e-4, -1.9e-3, -6.3e-4, -3.6e-4, -5.7e-3, -4.4e-3, 6.3e-3, -2.0e-3, -7.3e-4, -5.1e-4, -1.8e-4, 7.0e-6, 6.8e-6, -2.7e-4, -2.2e-5, -3.8e-5 -1.7e-3, -3.6e-4, -3.1e-4, -1.9e-3, -4.5e-4, -5.2e-4, -2.3e-3, -3.4e-4, -7.6e-4, -6.7e-3, -4.6e-3, 6.5e-3, -8.2e-4, -1.7e-4, -4.0e-5, -3.4e-4, 2.9e-5, -3.3e-5 -2.6e-4, 4.7e-6, -4.5e-5, -2.0e-4, 2.1e-5, -5.0e-5, -1.3e-4, 4.0e-5, -5.7e-5, -6.4e-4, -2.7e-4, -2.2e-4, -9.1e-3, -5.2e-3, 6.6e-3, -4.5e-3, -1.1e-3, -5.3e-4 -6.5e-4, -1.3e-4, -2.9e-4, -5.3e-4, -1.0e-4, -1.0e-4, -2.9e-4, 1.9e-5, -8.0e-5, -4.3e-4, 1.6e-5, -1.8e-5, -4.7e-3, -1.2e-3, -4.3e-4, -8.7e-3, -4.6e-3, 6.8e-3

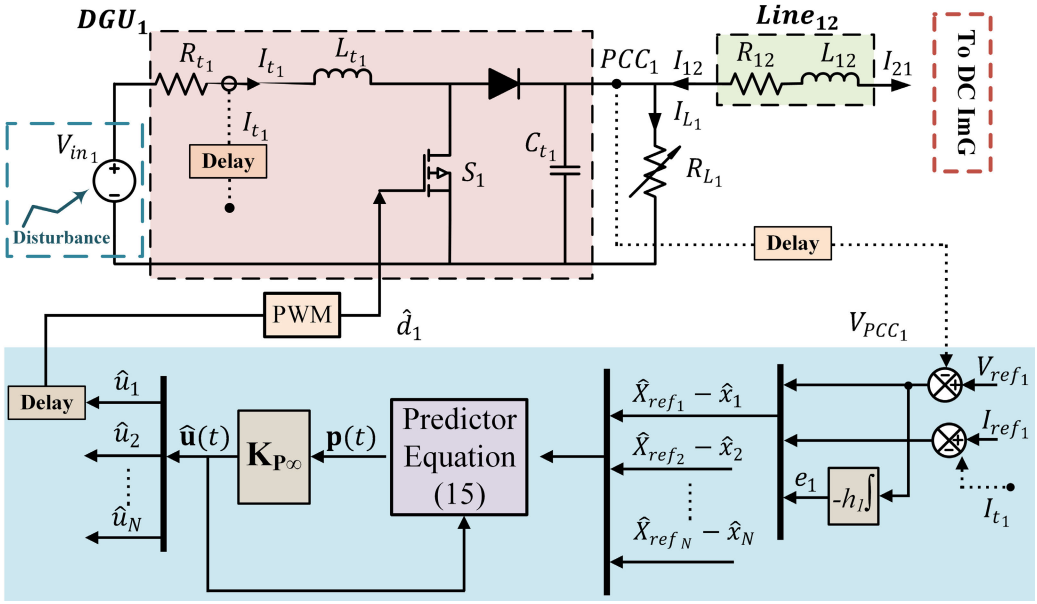

FIGURE 5. Predictor-based robust control architecture.

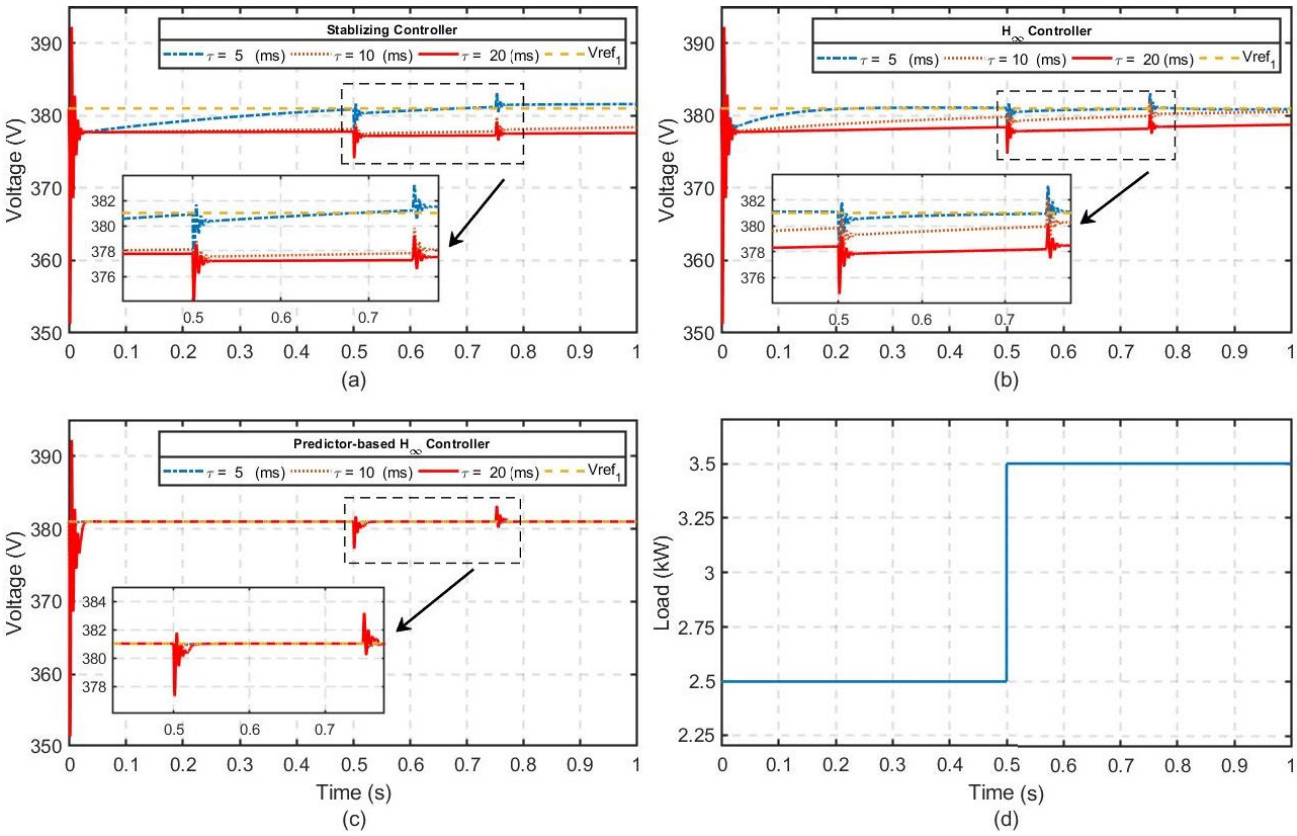

FIGURE 6. TDS controller performance against load increase at PCC_1.

Thus far, the input time-delay in the TDS system (10) is successfully eliminated, and the closed-loop system (19) is obtained by introducing a new fictitious disturbance vector. However, from the predictor-based control input (17), we find that the prediction vector is appended to the state vector; therefore, its dynamic must be considered, which is obtained as follows:

$$\dot{\mathbf{p}}(t) = e^{\hat{\mathbf{A}}\tau}\dot{\hat{\mathbf{x}}}(t) + \hat{\mathbf{B}}\hat{\mathbf{u}}(t) - e^{\hat{\mathbf{A}}\tau}\hat{\mathbf{B}}\hat{\mathbf{u}}(t-\tau) + \int_{t-\tau}^{t} \hat{\mathbf{A}}e^{\hat{\mathbf{A}}\tau}[\hat{\mathbf{B}}\hat{\mathbf{u}}(s)]ds \quad (20)$$

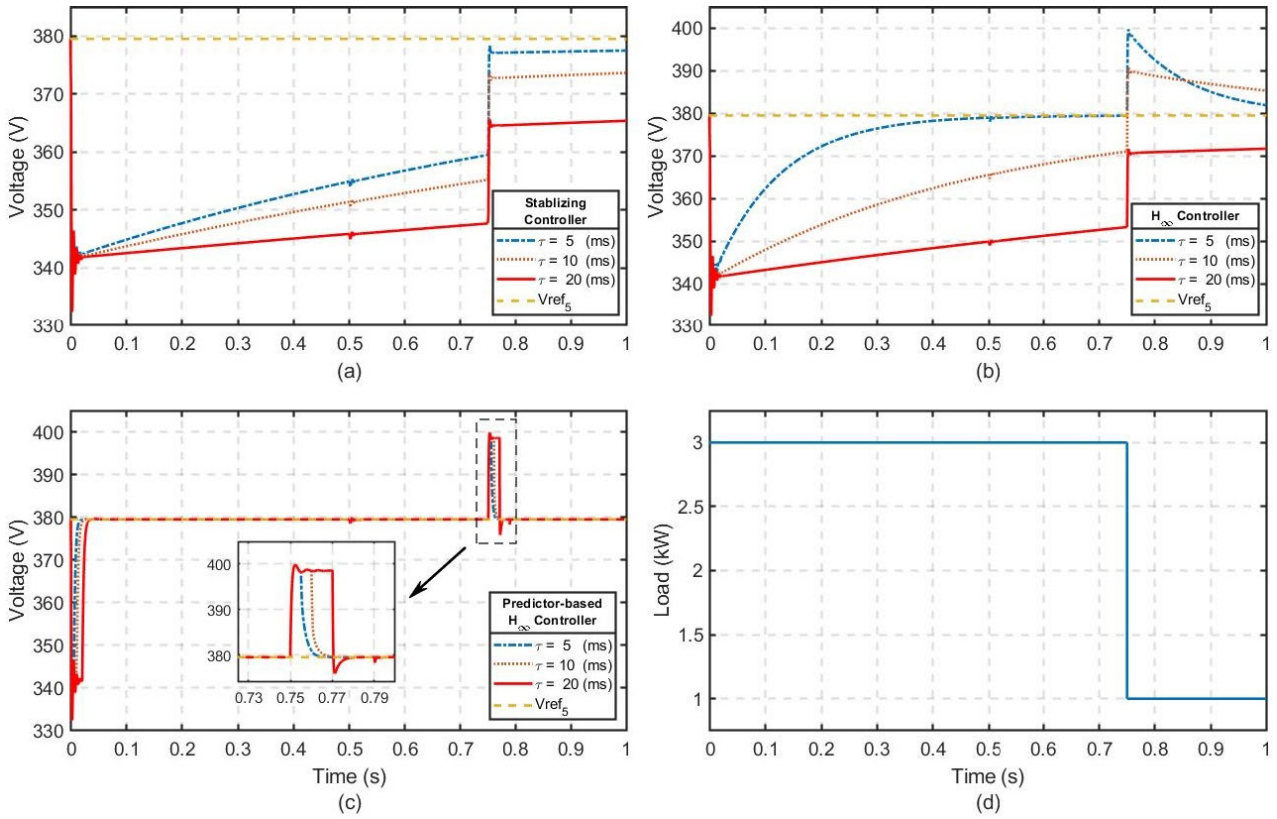

FIGURE 7. TDS controller performance against load decrease at PCC_5.

Substituting (10), (15), and (17) in (20), the differential equation of the prediction-vector is obtained as

$$\begin{aligned}\dot{\mathbf{p}}(t) &= (\hat{\mathbf{A}}+\hat{\mathbf{B}}\mathbf{K}_{P\infty})\hat{\mathbf{p}}(t)+e^{\hat{\mathbf{A}}\tau}\hat{\mathbf{D}}\hat{\mathbf{w}}(t)\\ &= (\hat{\mathbf{A}}+\hat{\mathbf{B}}\mathbf{K}_{P\infty})\hat{\mathbf{p}}(t)+\mathbf{D}_2\bar{\mathbf{w}}(t),\end{aligned} \tag{21}$$

where $\hat{\mathbf{A}}e^{\hat{\mathbf{A}}\tau}=e^{\hat{\mathbf{A}}\tau}\hat{\mathbf{A}}$, $\hat{\mathbf{D}}_2=\mathbf{M}[\hat{\mathbf{D}}\ \ \mathbf{0}]$, $\mathbf{M}=e^{\hat{\mathbf{A}}\tau}$ $\bar{\mathbf{w}}=[\hat{\mathbf{w}}^\top\ \ \tilde{\mathbf{w}}^\top]$, $\tilde{\mathbf{w}}^\top=-\mathbf{K}_{P\infty}\hat{\mathbf{e}}_p(t-\tau)$.

From the above, we can conclude that the stability of the TDS (10) with a prediction-based controller (17) is equivalent to the stability of two delay-less differential equations (19) and (21). At this stage, we are ready to introduce the main theorem of this paper, which provides the gain of the predictor-based controller.

Theorem 3: Assuming positive constants γ, β, and λ, the linear TDS (10) with the prediction-based controller (17) is asymptotically stable in the absence of exogenous disturbance, and in the presence of disturbance, it satisfies the $\mathcal{L}_2$-gain criterion $||\hat{\mathbf{z}}||^2_{\mathcal{L}_2} \leq \gamma^2\ ||\bar{\mathbf{w}}||^2_{\mathcal{L}_2}$ for $\bar{\mathbf{w}}(t) \in \mathcal{L}_2[0,\ \infty)$. The control input is limited $\hat{\mathbf{u}} \leq \bar{\mathbf{u}}$, if there exist symmetric positive definite matrices $\mathbf{X} > \mathbf{0}$ and $\mathbf{Y} > \mathbf{0}$ with appropriate dimensions, such that the following LMIs hold

$$\begin{bmatrix}\Psi_{11} & \mathbf{0} & \hat{\mathbf{D}} & \hat{\mathbf{B}} & \Psi_{15}\\ * & \Psi_{22} & \lambda\mathbf{M}\hat{\mathbf{D}} & \mathbf{0} & \mathbf{0}\\ * & * & -\gamma^2\mathbf{I} & \mathbf{0} & \mathbf{0}\\ * & * & * & -\gamma^2\mathbf{I} & \hat{\mathbf{D}}_{12}^\top\\ * & * & * & * & -\mathbf{I}\end{bmatrix} < \mathbf{0} \tag{22}$$

$$\begin{bmatrix}\beta\lambda\bar{\mathbf{u}}^2 & \mathbf{Y}^\top\\ \mathbf{Y} & \mathbf{I}\end{bmatrix} \geq \mathbf{0}, \tag{23}$$

where $\Psi_{11}=\mathbf{X}\hat{\mathbf{A}}^\top+\mathbf{Y}^\top\hat{\mathbf{B}}^\top+\hat{\mathbf{A}}\mathbf{X}+\hat{\mathbf{B}}\mathbf{Y}$, $\Psi_{15}=\mathbf{X}\hat{\mathbf{C}}_1^\top+\mathbf{Y}^\top\hat{\mathbf{D}}_{12}^\top$, $\Psi_{22}=\lambda(\mathbf{X}\hat{\mathbf{A}}^\top+\mathbf{Y}^\top\hat{\mathbf{B}}^\top+\hat{\mathbf{A}}\mathbf{X}+\hat{\mathbf{B}}\mathbf{Y})$, and the gain of the controller (17) is obtained by $\mathbf{K}_{P\infty}=\mathbf{Y}\mathbf{X}^{-1}$.

Proof 3: The proof of Theorem 3 is presented in Appendix C.

Remark: The prediction vector Equation (14) or (15) can be calculated from the past values inputs of τ *ms* and the and current state. The integral and the exponential term in Equation (15) can obtained by fast processor at each step which is then multiplied with the gain $\mathbf{K}_{P\infty}$.

IV. SIMULATION RESULTS

We now investigate the performance of the proposed controllers for the DC ImG comprising six DGUs, as depicted in Fig. 4. The electrical-parameters of the system are listed in Table 1. The control gains for the controller are obtained by solving the respective LMIs discussed in the last section using the YALMIP toolbox in MATLAB and Mosek as a solver [49], [50]. The controller's performance is tested for different communication delays against voltage-disturbances and load-disturbances.

To achieve the stabilizing controller gains $\mathbf{K}_s$, $\mathbf{K}_\infty$ and $\mathbf{K}_{P\infty}$ theorems 1, 2, and 3 are solved by considering the values in Table 2. The performance of the proposed controllers are checked for input-voltage disturbances and

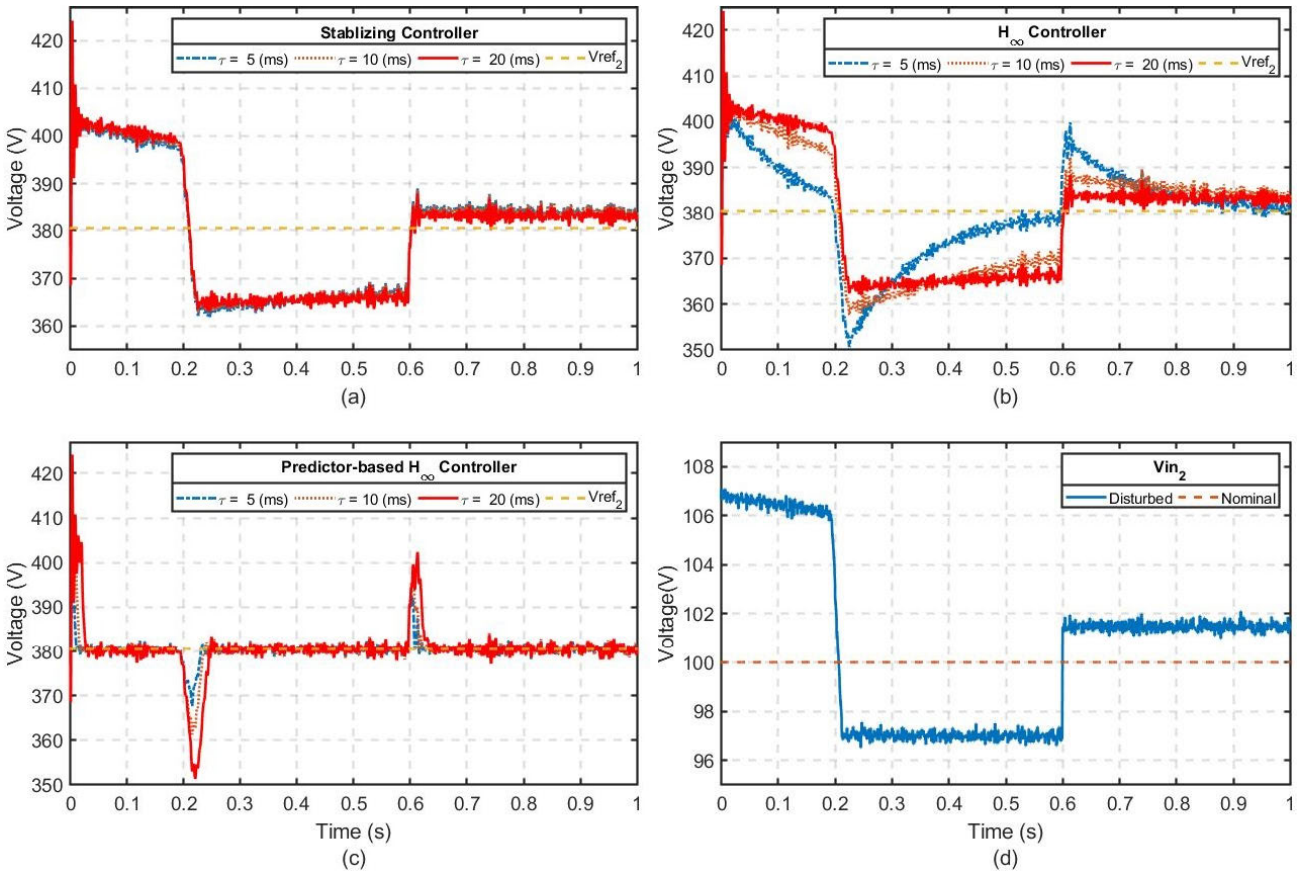

FIGURE 8. TDS controller performance against input-voltage variations for PCC_2.

load variations when there is a communication delay of 5 *ms*, 10 *ms*, and 20 *ms*. The controller gains are provided as Table 4 (see paper end). Where the gains are for the state as given in equation (5).

Feasibility of the stabilizing, robust, and predictor-based controllers for different delays are provided in Table 3. We find that the stabilizing and predictor-based controllers are feasible for all tested delay cases, however, the robust controller LMIs are feasible up to 20*ms* delay.

A. LOAD VARIATION CASE

To test the proposed TDS controllers' performance against load disturbances, the local loads of DGU_1 and DGU_5 of the DC ImG Fig. 4 are varied. The initial load of DGU_1 is $2.5kW$, and at $t = 0.5s$, it is increased to $3.5kW$. This load variation is illustrated in Fig. 6(d). The performance of the stabilizing, robust, and predictor-based robust controllers against increases in the load are depicted in Fig 6(a)–(c). We found that the stabilizing and H_∞ controllers are slow in tracking the reference voltage $Vref_1$ for the same error dynamic parameter h_i. Furthermore, we found that as the delay increases from 5*ms* to 20*ms*, the controllers' response further deteriorates. In contrast to the stabilizing and robust H_∞ controllers, the predictor-based robust H_∞ controller (Fig. 5) is almost unaffected because of load change and delay.

Similar to the load increase test, the proposed controllers have also been tested for the load decrease case, wherein for DGU_5, the local load is decreased to $1kW$ from an initial load of $3kW$ (Fig. 7(d)). The reference voltages $Vref_5$ tracking performance of the stabilizing, robust, and predictor-based robust controllers are depicted in Fig. 7(a)–(d). From the resulting plots, we observe that the performances of the stabilizing and the H_∞ controllers further deteriorate with the increase in communication delay. The load decrease scenario is handled exquisitely by the predictor-based robust controller in all delay cases.

All other *PCC* loads (Fig. 4) are maintained constant according to Table 1; therefore, their voltages are not included in the results. Furthermore, in Fig. 6(a)–(c), the second disturbance at $t = 0.75$ is due to the load decrease at PCC_5, as depicted in Fig. 7.

B. INPUT VOLTAGE VARIATION CASE

It is known that the typical *DGU* is an *RES* (e.g. PV-system), which has an intermittent nature and can be modeled as voltage variations [51]–[53]. This input-voltage variation is modelled as a disturbance $\tilde{v}_{in_i}$ in (1). Therefore, the proposed controllers' performance is tested against the input-voltage

Vin_i variations or disturbances. The variations in the input-voltage have two components, namely, the change in the source-voltage level and the noise. For the voltage level change, the input-voltage Vin_i is varied by $\pm 5\%$ of the nominal voltages listed in Table 1. This imitates the solar PV source behavior. The noise represents the small-signal voltage variations that are considered to be a $\pm 1V$ uniformly distributed stochastic process.

The performance of DGU_2 in the presence of input voltage disturbances is depicted in Fig. 8. In Fig. 8(d), the 'Nominal' and 'Disturbed' Vin_2 are depicted. The performances of the proposed TDS controllers for DGU_2 in this scenario are plotted in Fig. 8(a), (b), and (c). From the PCC_2 voltage, we observe that the stabilizing and robust controllers Fig. 8(a) and (b), respectively, transferred the input-voltage disturbances to the output voltage; therefore, these controllers could not maintain the $Vref_2$. However, the predictor-based robust controller performance is not affected adversely. This controller maintained the PCC_2 voltage up to an acceptable range.

V. CONCLUSION

In this study, the stability and control of DC ImG were studied with communication delays. For the DC ImG with communication delay, three control schemes were developed—stabilizing, robust, and predictor-based robust controllers. The stability of the time-delay DC ImG system was guaranteed by the selection of an appropriate Lyapunov-Krasovskii functional in each case. Whereas, the robustness of the robust controllers was achieved as per H_∞ disturbance attenuation criterion. The overall control problems were transformed into LMI convex optimization problems with constraints. The performances of these controllers were verified for the load variations and input voltage disturbances under three delay scenarios. The results demonstrated that among the three proposed TDS controllers, the predictor-based robust controller maintained good voltage regulation and system in all the test cases.

The future work of this research includes physical implementation of the predictor-based robust controller and its comparison with the similar research.

APPENDIXES

APPENDIX A

A. PROOF OF THEOREM 1

If in the system (5) or (7), the delay is a time-varying parameter, i.e., $\tau(t) \in [0, h]$, then the LKF for delay-dependent stability is a state derivative dependent on the form.

$$\begin{aligned}\mathbf{V}(t, \hat{\mathbf{x}}_t, \dot{\hat{\mathbf{x}}}_t) = \hat{\mathbf{x}}^\top(t)\mathbf{P}\hat{\mathbf{x}}(t) + \int_{t-h}^{t} \hat{\mathbf{x}}^\top(s)\mathbf{S}\hat{\mathbf{x}}(s)ds \\ + h\int_{-h}^{0}\int_{t+\theta}^{t} \dot{\hat{\mathbf{x}}}^\top(s)\mathbf{R}\dot{\hat{\mathbf{x}}}(s)ds d\theta \\ + \int_{t-\tau}^{t} \hat{\mathbf{x}}^\top(s)\mathbf{Q}\hat{\mathbf{x}}(s)ds, \end{aligned} \tag{24}$$

where $\mathbf{P} > \mathbf{0}, \mathbf{S} \geq \mathbf{0}, \mathbf{R} \geq \mathbf{0}, \mathbf{Q} \geq \mathbf{0}$.

Differentiating $\mathbf{V}$, we obtain the following expression

$$\begin{aligned}\dot{\mathbf{V}} = 2\hat{\mathbf{x}}^\top(t)\mathbf{P}\dot{\hat{\mathbf{x}}}(t) + h^2\dot{\hat{\mathbf{x}}}^\top(t)\mathbf{R}\dot{\hat{\mathbf{x}}}(t) - h\int_{t-h}^{t} \dot{\hat{\mathbf{x}}}^\top(s)\mathbf{R}\dot{\hat{\mathbf{x}}}(s)ds \\ + \hat{\mathbf{x}}^\top(t)[\mathbf{S}+\mathbf{Q}]\hat{\mathbf{x}}(t) - \hat{\mathbf{x}}^\top(t-h)\mathbf{S}(\hat{\mathbf{x}}(t-h) \\ - (1-\dot{\tau})\hat{\mathbf{x}}^\top(t-\tau(t))\mathbf{Q}\hat{\mathbf{x}}(t-\tau) \end{aligned} \tag{25}$$

Applying Jensen's inequality [44, p. 87] to the integral term in (25), we obtain

$$\begin{aligned}\dot{\mathbf{V}} \leq 2\hat{\mathbf{x}}^\top(t)\mathbf{P}\dot{\hat{\mathbf{x}}}(t) + h^2\dot{\hat{\mathbf{x}}}^\top(t)\mathbf{R}\dot{\hat{\mathbf{x}}} \\ - [\hat{\mathbf{x}}(t) - \hat{\mathbf{x}}(t-\tau)]^\top\mathbf{R}[\hat{\mathbf{x}}(t) - \hat{\mathbf{x}}(t-\tau] \\ - [\hat{\mathbf{x}}(t-\tau) - \hat{\mathbf{x}}(t-h)]^\top\mathbf{R}[\hat{\mathbf{x}}(t-\tau) - \hat{\mathbf{x}}(t-h)] \\ + \hat{\mathbf{x}}^\top(t)[\mathbf{S}+\mathbf{Q}]\hat{\mathbf{x}}(t) - \hat{\mathbf{x}}^\top(t-h)\mathbf{S}\hat{\mathbf{x}}^\top(t-h) \\ - (1-d)\hat{\mathbf{x}}^\top(t-\tau)\mathbf{Q}\hat{\mathbf{x}}(t-\tau) \end{aligned} \tag{26}$$

Hence, the LMI in (8) is obtained.

$$\bar{\Phi} = \begin{bmatrix} \bar{\phi}_{11} & \bar{\phi}_{12} & \bar{\mathbf{S}}_{12} & \bar{\phi}_{14} \\ * & \bar{\phi}_{22} & \mathbf{0} & \epsilon\hat{\mathbf{B}}\mathbf{Y} \\ * & * & -(\bar{\mathbf{S}}+\bar{\mathbf{R}}) & \bar{\mathbf{R}} - \bar{\mathbf{S}}_{12}^\top \\ * & * & * & \bar{\phi}_{44} \end{bmatrix} < \mathbf{0}, \tag{27}$$

where $\bar{\phi}_{ij}$ and other terms are as given in LMI (8).

Similarly, LMI (9) can be obtained by multiplying $\begin{bmatrix} \mathbf{R} & \mathbf{S}_{12} \\ * & \mathbf{R} \end{bmatrix} \geq \mathbf{0}$ by $diag\begin{pmatrix} \bar{\mathbf{P}}_2 & \bar{\mathbf{P}}_2 \end{pmatrix}$. Therefore, the proof is complete. □

APPENDIX B

B. PROOF OF THEOREM 2

Substituting the system (12), into the inequality (26) we get the $\mathcal{J}_\infty$ cost function

$$\mathcal{J}_\infty = \int_0^\infty \left(\hat{\mathbf{z}}^\top(t)\hat{\mathbf{z}}(t) - \gamma^2\hat{\mathbf{w}}(\mathbf{t})\hat{\mathbf{w}}(\mathbf{t}) + \dot{\hat{\mathbf{v}}}(t)\right) dt < \mathbf{0} \tag{28}$$

The $\mathcal{J}_\infty$ can be expressed as LMI (13). The detailed proof is available in [44, p. 150].

APPENDIX C

Before applying the proof of the theorem, we present an important mathematical lemma, which is used in the proof.

Lemma 5: (Schur complement) [44] For the matrices A, B, and C of appropriate dimensions, the following inequality holds:

$$\mathrm{M} = \begin{bmatrix} A & B \\ B^\top & C \end{bmatrix} > 0 \Longleftrightarrow A - BC^{-1}B^\top > 0, \text{ and } C > 0.$$

Here, the Schur complement of the matrix block C of M is expressed by the inequality $A - BC^{-1}B^\top > 0$.

C. PROOF OF THEOREM 3

Let us consider the quadratic Lyapunov functional $\mathbf{V}(t)$ for the closed-loop systems (19) and (21)

$$\begin{aligned}\mathbf{V}(t) &= \mathbf{V}_1(\hat{\mathbf{x}}(t)) + \mathbf{V}_2(\mathbf{p}(t)) \\ &= \hat{\mathbf{x}}^\top(t)\mathbf{Q}_1\hat{\mathbf{x}}(t) + \mathbf{p}^\top(t)\mathbf{Q}_2\mathbf{p}(t), \end{aligned} \tag{29}$$

where $\mathbf{Q}_1 > \mathbf{0}$, $\mathbf{Q}_2 > \mathbf{0}$. Differentiating (29), we obtain

$$\dot{\mathbf{V}}(t) = \dot{\mathbf{V}}_1(\hat{\mathbf{x}}(t)) + \dot{\mathbf{V}}_2(\mathbf{p}(t)), \tag{30}$$

where

$$\begin{aligned}
\dot{\mathbf{V}}_1 &= \dot{\hat{\mathbf{x}}}^\top(t)\mathbf{Q}_1\hat{\mathbf{x}}(t) + \hat{\mathbf{x}}^\top(t)\mathbf{Q}_1\dot{\hat{\mathbf{x}}}(t) \\
&= \hat{\mathbf{x}}^\top(t)(\hat{\mathbf{A}} + \hat{\mathbf{B}}\mathbf{K}_{P\infty})^\top\mathbf{Q}_1\hat{\mathbf{x}}(t) + \bar{\mathbf{w}}^\top(t)\mathbf{D}_1^\top\mathbf{Q}_1\hat{\mathbf{x}}(t) \\
&\quad + \hat{\mathbf{x}}^\top(t)\mathbf{Q}_1(\hat{\mathbf{A}} + \hat{\mathbf{B}}\mathbf{K}_{P\infty})\hat{\mathbf{x}}(t) + \hat{\mathbf{x}}^\top(t)\mathbf{Q}_1\mathbf{D}_1\bar{\mathbf{w}}(t), \\
\dot{\mathbf{V}}_2 &= \dot{\mathbf{p}}^\top(t)\mathbf{Q}_2\mathbf{p}(t) + \mathbf{p}^\top(t)\mathbf{Q}_2\dot{\mathbf{p}}(t) \\
&= \mathbf{p}^\top(t)(\hat{\mathbf{A}} + \hat{\mathbf{B}}\mathbf{K}_{P\infty})^\top\mathbf{Q}_2\mathbf{p}(t) + \bar{\mathbf{w}}^\top(t)\mathbf{D}_2^\top\mathbf{Q}_2\mathbf{p}(t) \\
&\quad + \mathbf{p}^\top(t)\mathbf{Q}_2(\hat{\mathbf{A}} + \hat{\mathbf{B}}\mathbf{K}_{P\infty})\mathbf{p}(t) + \mathbf{p}^\top(t)\mathbf{Q}_2\mathbf{D}_2\bar{\mathbf{w}}(t),
\end{aligned}$$

Define $\zeta = [\hat{\mathbf{x}}^\top(t) \quad \mathbf{p}^\top(t) \quad \bar{\mathbf{w}}^\top(t)]^\top$ and rewriting (29) as $\dot{\mathbf{V}}(t) = \zeta^\top \Xi \zeta$, the stability criterion can be expressed as

$$\Xi = \begin{bmatrix} \Phi_{11} & \mathbf{0} & \mathbf{Q}_1\mathbf{D}_1 \\ * & \Phi_{22} & \mathbf{Q}_2\mathbf{D}_2 \\ * & * & \mathbf{0} \end{bmatrix} < \mathbf{0}, \tag{31}$$

where

$$\begin{aligned}
\Phi_{11} &= (\hat{\mathbf{A}} + \hat{\mathbf{B}}\mathbf{K}_{P\infty})^\top\mathbf{Q}_1 + \mathbf{Q}_1(\hat{\mathbf{A}} + \hat{\mathbf{B}}\mathbf{K}_{P\infty}) \\
\Phi_{22} &= (\hat{\mathbf{A}} + \hat{\mathbf{B}}\mathbf{K}_{P\infty})^\top\mathbf{Q}_2 + \mathbf{Q}_2(\hat{\mathbf{A}} + \hat{\mathbf{B}}\mathbf{K}_{P\infty})
\end{aligned}$$

Assuming at initial condition $\hat{\mathbf{u}}(t) = \phi(t) = 0, \forall\, t \in [-\tau\ 0]$ we have $\mathbf{V}(t)|_{t=0} = \mathbf{0}$. Consider the cost $\mathcal{J}_{P\infty}$.

$$\begin{aligned}
\mathcal{J}_{P\infty} &= \int_0^\infty \left(\hat{\mathbf{z}}^\top(t)\hat{\mathbf{z}}(t) - \gamma^2\bar{\mathbf{w}}^\top(t)\bar{\mathbf{w}}(t) + \dot{\hat{\mathbf{V}}}(t)\right) dt < \mathbf{0} \\
&= \int_0^\infty \zeta^\top\ \Pi_1\ \zeta dt < \mathbf{0},
\end{aligned} \tag{32}$$

where ζ is as defined in (31),

$$\Pi_1 = \begin{bmatrix} \Pi_{11} & \mathbf{0} & \Pi_{13} \\ * & \Phi_{22} & \mathbf{Q}_2\mathbf{D}_2 \\ * & * & \bar{\mathbf{D}}_{12}^\top\bar{\mathbf{D}}_{\mathbf{12}} - \gamma^2\mathbf{I}, \end{bmatrix} \tag{33}$$

where

$$\begin{aligned}
\Pi_{11} &= \Phi_{11} + (\hat{\mathbf{C}} + \hat{\mathbf{D}}_{12}\mathbf{K}_{P\infty})^\top(\hat{\mathbf{C}} + \hat{\mathbf{D}}_{12}\mathbf{K}_{P\infty}) \\
\Pi_{13} &= \mathbf{Q}_1\hat{\mathbf{D}}_1 + \mathbf{Q}_2(\hat{\mathbf{C}} + \hat{\mathbf{D}}_{12}\mathbf{K}_{P\infty})^\top\bar{\mathbf{D}}_{\mathbf{12}}
\end{aligned}$$

With zero-exogenous disturbance, i.e., $\bar{\mathbf{w}}(t) = \mathbf{0}$, if (33) is a negative definite, then $\dot{\mathbf{V}} < \mathbf{0}$, and from Lyapunov stability criterion, the TDS (10) is asymptotically stable. Applying Schur Lemma 5 on (33), we obtain

$$\Pi_2 = \begin{bmatrix} \Phi_{11} & \mathbf{0} & \mathbf{Q}_1\mathbf{D}_1 & \begin{pmatrix} \hat{\mathbf{C}} + \\ \hat{\mathbf{D}}_{12}\mathbf{K}_{P\infty} \end{pmatrix}^\top \\ * & \Phi_{22} & \mathbf{Q}_2\mathbf{D}_2 & \mathbf{0} \\ * & * & -\gamma^2\mathbf{I} & \bar{\mathbf{D}}_{12}^\top \\ * & * & * & -\mathbf{I} \end{bmatrix} < \mathbf{0} \tag{34}$$

Substituting $\mathbf{D}_1 = [\hat{\mathbf{D}} \quad \hat{\mathbf{B}}]$, $\bar{\mathbf{D}}_{\mathbf{12}} = [\mathbf{0} \quad \hat{\mathbf{D}}_{12}]$, and $\mathbf{D}_2 = [\hat{\mathbf{D}}\ \mathbf{0}]$, then

$$\Pi_2 = \begin{bmatrix} \Phi_{11} & \mathbf{0} & \mathbf{Q}_1\hat{\mathbf{D}} & \mathbf{Q}_1\mathbf{B} & \begin{pmatrix} \hat{\mathbf{C}} + \\ \hat{\mathbf{D}}_{12}\mathbf{K}_{P\infty} \end{pmatrix}^\top \\ * & \Phi_{22} & \mathbf{Q}_2\mathbf{M}\hat{\mathbf{D}} & \mathbf{0} & \mathbf{0} \\ * & * & -\gamma^2\mathbf{I} & \mathbf{0} & \mathbf{0} \\ * & * & * & -\gamma^2\mathbf{I} & \hat{\mathbf{D}}_{12}^\top \\ * & * & * & * & -\mathbf{I} \end{bmatrix} < \mathbf{0} \tag{35}$$

Let $\mathbf{Q}_2 = \lambda\mathbf{Q}_1$. By multiplying (35) by $diag(\mathbf{Q}_1^{-1}, \mathbf{Q}_1^{-1}, \mathbf{I}, \mathbf{I}, \mathbf{I})$ and its transpose on both sides respectively, we obtain the following

$$\Pi_3 = \begin{bmatrix} \Psi_{11} & \mathbf{0} & \hat{\mathbf{D}} & \hat{\mathbf{B}} & \Psi_{15} \\ * & \Psi_{22} & \lambda\mathbf{M}\hat{\mathbf{D}} & \mathbf{0} & \mathbf{0} \\ * & * & -\gamma^2\mathbf{I} & \mathbf{0} & \mathbf{0} \\ * & * & * & -\gamma^2\mathbf{I} & \hat{\mathbf{D}}_{12}^\top \\ * & * & * & * & -\mathbf{I} \end{bmatrix} < \mathbf{0} \tag{36}$$

Hence, the LMI in (22) is obtained.

Thus far, we have derived the conditions for the existence of the gain-matrix $\mathbf{K}_{P\infty}$ that guarantees the asymptotic stability of the closed-loop TDS. Now, we provide the condition under which we reduce the control input $\hat{\mathbf{u}}(t) = \mathbf{K}_{P\infty}\mathbf{p}(t)$ effort in (17).

Given $\dot{\mathbf{V}}(t) \leq \mathbf{0}$ (29) holds for the TDS (10). Then, $\mathbf{p}^\top(t)\mathbf{Q}_2\mathbf{p}(t) \leq \mathbf{p}_0^\top\mathbf{Q}_2\mathbf{p}_0$ for $t \geq 0$, i.e., the ellipsoid $\mathcal{H} = \{\mathbf{p}_0 \in \mathbb{R}^N : \mathbf{p}_0^\top\mathbf{Q}_2\mathbf{p}_0 \leq \beta^{-1}\}$ for any $\beta > 0$ is a positive invariant for the system: The system (10) starting from $\mathbf{p}_0 \in \mathcal{H}$ remains in $\mathcal{H}$ $\forall\ t \geq 0$. Additionally, the following implication holds:

$$\mathbf{p}^\top(t)\mathbf{Q}_2\mathbf{p}(t) \leq \beta^{-1} \implies \mathbf{p}^\top(t)\mathbf{K}_{P\infty}^\top\mathbf{K}_{P\infty}\mathbf{p}(t) \leq \bar{\mathbf{u}}^2(t), \tag{37}$$

where $\hat{\mathbf{u}}(t) \leq \bar{\mathbf{u}}(t)$. Then,

$$\mathbf{p}^\top(t)\mathbf{K}_{P\infty}^\top\mathbf{K}_{P\infty}\mathbf{p}(t) \leq \beta\mathbf{p}^\top(t)\mathbf{Q}_2\mathbf{p}(t)\bar{\mathbf{u}}^2(t) \tag{38}$$

Applying Schur Lemma 5, we obtain

$$\begin{bmatrix} \beta\mathbf{Q}_2\bar{\mathbf{u}}^2 & \mathbf{K}_{P\infty}^\top \\ \mathbf{K}_{P\infty} & \mathbf{I} \end{bmatrix} \geq \mathbf{0} \tag{39}$$

By pre- and post-multiplying the above equation by $diag(\mathbf{Q}_1^{-1}, \mathbf{I})$ and its transpose from both sides, we obtain

$$\begin{bmatrix} \beta\mathbf{Q}_1^{-1}\mathbf{Q}_2\bar{\mathbf{u}}^2 & \mathbf{Q}_1^{-1}\mathbf{K}_{P\infty}^\top \\ \mathbf{K}_{P\infty}\mathbf{Q}_1^{-1} & \mathbf{I} \end{bmatrix} \begin{bmatrix} \mathbf{Q}^{-1} & \mathbf{0} \\ \mathbf{0} & \mathbf{I} \end{bmatrix} \geq \mathbf{0} \tag{40}$$

$$\begin{bmatrix} \beta\lambda\bar{\mathbf{u}}^2 & \mathbf{Y}^\top \\ \mathbf{Y} & \mathbf{I} \end{bmatrix} \geq \mathbf{0} \tag{41}$$

Hence, the LMI for limiting the control effort in (23) is obtained. Therefore, the proof is complete. □

REFERENCES

[1] E. Pritchard and D. C. Gregory, "The DC revolution [viewpoint]," *IEEE Electrific. Mag.*, vol. 4, no. 2, pp. 4–9, Jun. 2016.

[2] L. E. Zubieta, "Are microgrids the future of energy?: DC microgrids from concept to demonstration to deployment," *IEEE Electrific. Mag.*, vol. 4, no. 2, pp. 37–44, Jun. 2016.

[3] A. T. Elsayed, A. A. Mohamed, and O. A. Mohammed, "DC microgrids and distribution systems: An overview," *Electric Power Syst. Res.*, vol. 119, pp. 407–417, Feb. 2015.

[4] Y. Han, X. Ning, P. Yang, and L. Xu, "Review of power sharing, voltage restoration and stabilization techniques in hierarchical controlled DC microgrids," *IEEE Access*, vol. 7, pp. 149202–149223, 2019.

[5] G. S. Rawat and Sathans, "Survey on DC microgrid architecture, power quality issues and control strategies," in *Proc. 2nd Int. Conf. Inventive Syst. Control (ICISC)*, Jan. 2018, pp. 500–505.

[6] K. M. Bhargavi and N. S. Jayalakshmi, "A new control strategy for plug-in electric vehicle of DC microgrid with PV and wind power integration," *J. Electr. Eng. Technol.*, vol. 14, no. 1, pp. 13–25, Jan. 2019.

[7] D. O'Keeffe, S. Riverso, L. Albiol-Tendillo, and G. Lightbody, "Voltage control of DC islanded microgrids: Scalable decentralised L1 adaptive controllers," 2018, *arXiv:1801.04508*. [Online]. Available: http://arxiv.org/abs/1801.04508

[8] M. Kim, S. Lee, and S. Bae, "Decentralized power management for electrical power systems in more electric aircrafts," *Electronics*, vol. 7, no. 9, p. 187, 2018.

[9] A. Oulis Rousis, D. Tzelepis, I. Konstantelos, C. Booth, and G. Strbac, "Design of a hybrid AC/DC microgrid using HOMER pro: Case study on an islanded residential application," *Inventions*, vol. 3, no. 3, p. 55, 2018.

[10] A. Shekhar, L. Ramirez-Elizondo, and P. Bauer, "DC microgrid islands on ships," in *Proc. IEEE 2nd Int. Conf. DC Microgrids (ICDCM)*, Jun. 2017, pp. 111–118.

[11] M. S. Sadabadi, Q. Shafiee, and A. Karimi, "Plug-and-Play robust voltage control of DC microgrids," *IEEE Trans. Smart Grid*, vol. 9, no. 6, pp. 6886–6896, Nov. 2018.

[12] C. Dou, D. Yue, J. M. Guerrero, X. Xie, and S. Hu, "Multiagent system-based distributed coordinated control for radial DC microgrid considering transmission time delays," *IEEE Trans. Smart Grid*, vol. 8, no. 5, pp. 2370–2381, Sep. 2017.

[13] M. Tucci, S. Riverso, J. C. Vasquez, J. M. Guerrero, and G. Ferrari-Trecate, "A decentralized scalable approach to voltage control of DC islanded microgrids," *IEEE Trans. Control Syst. Technol.*, vol. 24, no. 6, pp. 1965–1979, Nov. 2016.

[14] Y.-C. Jeung, D. D. Le, and D.-C. Lee, "Analysis and design of DC-bus voltage controller of energy storage systems in DC microgrids," *IEEE Access*, vol. 7, pp. 126696–126708, 2019.

[15] T. Dragičević, X. Lu, J. C. Vasquez, and J. M. Guerrero, "DC microgrids—Part II: A review of power architectures, applications, and standardization issues," *IEEE Trans. Power Electron.*, vol. 31, no. 5, pp. 3528–3549, May 2016.

[16] T. Dragičević, X. Lu, J. C. Vasquez, and J. M. Guerrero, "DC microgrids—Part I: A review of control strategies and stabilization techniques," *IEEE Trans. Power Electron.*, vol. 31, no. 7, pp. 4876–4891, Jul. 2016.

[17] D. Xie, L. Zhang, C. Gu, and Y. Li, "The steady-state analysis of DC distribution network embedded droop control and power flow controller," *J. Electr. Eng. Technol.*, vol. 14, no. 6, pp. 2225–2238, Nov. 2019.

[18] N. H. Van Der Blij, L. M. Ramirez-Elizondo, M. T. J. Spaan, and P. Bauer, "Stability and decentralized control of plug-and-play DC distribution grids," *IEEE Access*, vol. 6, pp. 63726–63736, 2018.

[19] C. Dou, D. Yue, Z. Zhang, and K. Ma, "MAS-based distributed cooperative control for DC microgrid through switching topology communication network with time-varying delays," *IEEE Syst. J.*, vol. 13, no. 1, pp. 615–624, Mar. 2019.

[20] Q. Ouyang, Z. Wang, K. Liu, G. Xu, and Y. Li, "Optimal charging control for lithium-ion battery packs: A distributed average tracking approach," *IEEE Trans. Ind. Informat.*, vol. 16, no. 5, pp. 3430–3438, May 2020.

[21] Q. Ouyang, J. Chen, J. Zheng, and H. Fang, "Optimal multiobjective charging for lithium-ion battery packs: A hierarchical control approach," *IEEE Trans. Ind. Informat.*, vol. 14, no. 9, pp. 4243–4253, Sep. 2018.

[22] K. Liu, K. Li, and C. Zhang, "Constrained generalized predictive control of battery charging process based on a coupled thermoelectric model," *J. Power Sour.*, vol. 347, pp. 145–158, Apr. 2017.

[23] T. Murakami and A. Fujinuma, "Ubiquitous networking: Towards a new paradigm," Nomura Res. Inst., Tokyo, Japan, NRI Paper 2, 2000.

[24] L. Meng, Q. Shafiee, G. Ferrari Trecate, H. Karimi, D. Fulwani, X. Lu, and J. M. Guerrero, "Review on control of DC microgrids and multiple microgrid clusters," *IEEE J. Emerg. Sel. Topics Power Electron.*, vol. 5, no. 3, pp. 928–948, Sep. 2017.

[25] M. Mehdi, S. Z. Jamali, M. O. Khan, S. Baloch, and C.-H. Kim, "Robust control of a DC microgrid under parametric uncertainty and disturbances," *Electric Power Syst. Res.*, vol. 179, Feb. 2020, Art. no. 106074.

[26] M. Mehdi, M. Saad, S. Z. Jamali, and C.-H. Kim, "Output-feedback based robust controller for uncertain DC islanded microgrid," *Trans. Inst. Meas. Control*, vol. 42, no. 6, pp. 1239–1251, Apr. 2020.

[27] A. G. Tsikalakis and N. D. Hatziargyriou, "Centralized control for optimizing microgrids operation," *IEEE Trans. Energy Convers.*, vol. 23, no. 1, pp. 241–248, Mar. 2008.

[28] J. Lai, X. Lu, X. Yu, W. Yao, J. Wen, and S. Cheng, "Distributed voltage control for DC mircogrids with coupling delays & noisy disturbances," in *Proc. 43rd Annu. Conf. IEEE Ind. Electron. Soc. (IECON)*, Oct. 2017, pp. 2461–2466.

[29] V. Nasirian, S. Moayedi, A. Davoudi, and F. L. Lewis, "Distributed cooperative control of DC microgrids," *IEEE Trans. Power Electron.*, vol. 30, no. 4, pp. 2288–2303, Apr. 2015.

[30] W. Jiang, C. Yang, Z. Liu, M. Liang, P. Li, and G. Zhou, "A hierarchical control structure for distributed energy storage system in DC micro-grid," *IEEE Access*, vol. 7, pp. 128787–128795, 2019.

[31] V. Nasirian, A. Davoudi, F. L. Lewis, and J. M. Guerrero, "Distributed adaptive droop control for DC distribution systems," *IEEE Trans. Energy Convers.*, vol. 29, no. 4, pp. 944–956, Dec. 2014.

[32] H. Liang, B. J. Choi, W. Zhuang, and X. Shen, "Stability enhancement of decentralized inverter control through wireless communications in microgrids," *IEEE Trans. Smart Grid*, vol. 4, no. 1, pp. 321–331, Mar. 2013.

[33] A. Asheibi, A. Khalil, A. M. Elbreki, Z. Rajab, A. Alfergani, A. Mohamed, and A. Nouh, "Stability analysis of PV-based DC microgrid with communication delay," in *Proc. 9th Int. Renew. Energy Congr. (IREC)*, Mar. 2018, pp. 1–6.

[34] B. Chaudhuri, R. Majumder, and B. C. Pal, "Wide-area measurement-based stabilizing control of power system considering signal transmission delay," *IEEE Trans. Power Syst.*, vol. 19, no. 4, pp. 1971–1979, Nov. 2004.

[35] H. Wu, K. S. Tsakalis, and G. T. Heydt, "Evaluation of time delay effects to wide-area power system stabilizer design," *IEEE Trans. Power Syst.*, vol. 19, no. 4, pp. 1935–1941, Nov. 2004.

[36] M. Dong, L. Li, Y. Nie, D. Song, and J. Yang, "Stability analysis of a novel distributed secondary control considering communication delay in DC microgrids," *IEEE Trans. Smart Grid*, vol. 10, no. 6, pp. 6690–6700, Nov. 2019.

[37] Y. Nie, M. Dong, W. Yuan, J. Yang, and Z. Liu, "Delay-dependent stability analysis of DC microgrid with distributed control considering communication delay," in *Proc. Chin. Autom. Congr. (CAC)*, Oct. 2017, pp. 7646–7651.

[38] C. Dou, D. Yue, Z. Zhang, and J. M. Guerrero, "Hierarchical delay-dependent distributed coordinated control for DC ring-bus microgrids," *IEEE Access*, vol. 5, pp. 10130–10140, 2017.

[39] L. Guo, Y. Feng, X. Li, C. Wang, and Y. Li, "Stability analysis of a DC microgrid with master-slave control structure," in *Proc. IEEE Energy Convers. Congr. Exposit. (ECCE)*, Sep. 2014, pp. 5682–5689.

[40] H. Hua, C. Hao, Y. Qin, and J. Cao, "Stochastic robust H_∞ control strategy for coordinated frequency regulation in energy Internet considering time delay and uncertainty," in *Proc. 13th World Congr. Intell. Control Autom. (WCICA)*, Jul. 2018, pp. 111–118.

[41] X. Lu, J. M. Guerrero, K. Sun, and J. C. Vasquez, "An improved droop control method for DC microgrids based on low bandwidth communication with DC bus voltage restoration and enhanced current sharing accuracy," *IEEE Trans. Power Electron.*, vol. 29, no. 4, pp. 1800–1812, Apr. 2014.

[42] J. He and Y. W. Li, "Analysis, design, and implementation of virtual impedance for power electronics interfaced distributed generation," *IEEE Trans. Ind. Appl.*, vol. 47, no. 6, pp. 2525–2538, Nov. 2011.

[43] Y. Wei Li and C.-N. Kao, "An accurate power control strategy for power-electronics-interfaced distributed generation units operating in a low-voltage multibus microgrid," *IEEE Trans. Power Electron.*, vol. 24, no. 12, pp. 2977–2988, Dec. 2009.

[44] E. Fridman, *Introduction to Time-Delay Systems: Analysis and Control*. Cham, Switzerland: Springer, 2014.

[45] E.-K. Boukas and Z.-K. Liu, *Deterministic and Stochastic Time-Delay Systems*. Springer, 2002.

[46] R. W. Erickson and D. Maksimovic, *Fundamentals of Power Electronics*. Springer, 2007.

[47] K. Karim Afshar, A. Javadi, and M. R. Jahed-Motlagh, "Robust H_∞ control of an active suspension system with actuator time delay by predictor feedback," *IET Control Theory Appl.*, vol. 12, no. 7, pp. 1012–1023, May 2018.
[48] K. Gu, "An integral inequality in the stability problem of time-delay systems," in *Proc. 39th IEEE Conf. Decis. Control*, vol. 3, Dec. 2000, pp. 2805–2810.
[49] J. Lofberg, "YALMIP : A toolbox for modeling and optimization in MATLAB," in *Proc. IEEE Int. Conf. Robot. Autom.*, Sep. 2004, pp. 284–289.
[50] A. Mosek, *MOSEK Optimization Toolbox for MATLAB*, document Release 9.0.104, 2019.
[51] M. Karimi, H. Mokhlis, K. Naidu, S. Uddin, and A. H. A. Bakar, "Photovoltaic penetration issues and impacts in distribution network—A review," *Renew. Sustain. Energy Rev.*, vol. 53, pp. 594–605, Jan. 2016.
[52] J.-P. Sawicki, F. Saint-Eve, P. Petit, F. Maufay, and M. Aillerie, "PV voltage control in spite of disturbances on MCB boost output voltage in parallel association," *Energy Procedia*, vol. 119, pp. 916–929, Jul. 2017.
[53] O. P. Mahela and S. R. Ola, "Impact of grid disturbances on the output of grid connected solar photovoltaic system," in *Proc. IEEE Students' Conf. Electr., Electron. Comput. Sci. (SCEECS)*, Mar. 2016, pp. 1–6.

MUHAMMAD MEHDI received the B.S. degree in electronic engineering from the Balochistan University of Information Technology, Engineering and Management Sciences (BUITEMS), Pakistan, in 2008, the M.Sc. degree in electrical engineering from the University of Engineering and Technology Lahore, Pakistan, in 2011, and the Ph.D. degree in electrical engineering from Sungkyunkwan University, South Korea, in 2020.

From 2011 to 2014, he worked with the Power Planning Division, National Transmission and Despatch Company Ltd., Pakistan, where he worked on the load flow analysis, power system stability, transmission planning, and electrical demand forecasting projects. In 2014, he joined BUITEMS as a Faculty Member. His research interests include power system dynamics, stability, and control in dc and ac microgrids.

CHUL-HWAN KIM (Senior Member, IEEE) received the B.S., M.S., and Ph.D. degrees in electrical engineering from Sungkyunkwan University, South Korea, in 1982, 1984, and 1990, respectively.

In 1990, he joined Cheju National University, Cheju, South Korea, as a full-time Lecturer. He was a Visiting Academic with the University of Bath, Bath, U.K., in 1996, 1998, and 1999. He has been a Professor with the College of Information and Computer Engineering, Sungkyunkwan University, since 1992, where he is currently the Director of the Center for Power Information Technology. His current research interests include power system protection, artificial intelligence applications for protection and control, modeling/protection of underground cable, and electromagnetic transients program software.

MUHAMMAD SAAD (Graduate Student Member, IEEE) received the B.Sc. degree from the University of Engineering and Technology, in 2015, and the M.S. degree from the National University of Sciences and Technology, Pakistan, in 2018. He is currently pursuing the Ph.D. degree with Sungkyunkwan University, South Korea. His research interests include robust observer-based power system fault estimation and islanding detection.